# A Multiscale Approach for Gas Hydrates Considering Structure, Agglomeration, and Transportability under Multiphase Flow Conditions: III. Agglomeration Model

Carlos Lange-Bassani, Celina Kakitani, Jean-Michel Herri, Amadeu K. Sum, Rigoberto E. M. Morales, Ana Cameirão

# A Multiscale Approach for Gas Hydrates Considering Structure, Agglomeration, and Transportability under Multiphase Flow Conditions: III. Agglomeration Model

*Carlos L. Bassani*[†,‡], *Celina Kakitani*[‡], *Jean-Michel Herri*[†], *Amadeu K. Sum*[#*], *Rigoberto E.M. Morales*[‡*], *Ana Cameirão*[†*]

[†]Mines Saint-Etienne, Univ Lyon, CNRS, UMR 5307 LGF, Centre SPIN, Departement PEG, F - 42023 Saint-Etienne France

[‡]Multiphase Flow Research Center (NUEM), Federal University of Technology – Paraná (UTFPR), Rua Deputado Heitor Alencar Furtado, 5000, Bloco N, CEP 81280-340, Curitiba/PR, Brazil

[#]Phases to Flow Laboratory, Chemical and Biological Engineering Department, Colorado School of Mines, 1500 Illinois St., Golden, CO 80401, USA

**Abstract**

In the third part of this series, we introduce the mathematical model for the agglomeration of gas hydrate in oil continuous flow. The aim is to develop an expression for the agglomeration efficiency that considers the existence of a wet or a dry particle. If the particle is wet, then water is available at its outer surface, thus allowing the formation of a liquid bridge that holds the aggregate together. The criterion for a wet or dry particle was developed in part II of this series and comes from the competitions between water permeation through the porous hydrate particle, and water consumption caused by crystallization in the particle's outer surface. The new expression for the agglomeration efficiency is coupled with a population balance solved through the Method of Moments and considering simple expressions for the collision rate and the shear rate induced by the flow coming from Smoluchowski's and Kolmogorov's theory, respectively. When compared to experimental data, the model stays within the ±40% deviation range and shows capable of predicting smaller agglomerate size for higher subcooling and lower interfacial properties (use of surfactant additives). The influence of subcooling into changing the porous medium parameters (especially the porous medium interconnectivity) shows to be important into the determination of the time taken for the particle to dry out. The model is simplified for engineering purposes considering gases much more soluble in oil than in water (hydrocarbon gases) in oil-continuous flow, and a simple criterion is proposed to predict if the system behaves as dispersed (slurry) or if it agglomerates after the onset of hydrate formation.

**Keywords**: flow assurance, gas hydrates, agglomeration, liquid bridge, population balance.

## 1. Introduction

This series is intended to describe both physically and mathematically the process of hydrate formation and agglomeration under multiphase flow by considering size-scales much smaller than the ones being currently adopted in literature. Part I[1] focused on the description of the phenomena based on the particle morphology (the called *sponge approach*) that leads to different interpretations of the growth kinetics (occurring at the capillary walls), and the agglomeration process (related to the particle being *wet or dry* and to the influence of surfactant additives in the entrapment of oil into the porous particles). Part II[2] describes mathematically the growth kinetics occurring in the outer surface of the particle and in the capillary walls, coupled with resistances due to gas absorption by the bulk and particle-bulk mass transfer (both concluded to be negligible when the gas is much more soluble in oil than in water, that is, hydrocarbon gases, and when oil is the continuous phase). In this article, part III, we describe the mathematical model of the agglomeration process. The reader is invited to read sections 2.3 and 2.4 of part I[1] (especially regarding Figures 8, 10 and 11) for a better comprehension of the agglomeration phenomena that will be herein modeled.

The modeling of agglomeration comes from the solution of the population balance, for which only a few studies exist applied to gas hydrates. The majority of them is for systems without oil. The first population balance applied to gas hydrates was done by Englezos et al.[3], using the Method of Moments, but only considering nucleation and growth. Herri et al.[4] expanded the model by considering agglomeration and breakage terms, where the collision rate of Smoluchowski[5] for a constant shear rate was coupled with an agglomeration efficiency based on electrostatic forces around the particle (DLVO theory) from van de Ven and Mason[6]. Balakin et al.[7–9] presented contributions in the solution of the population balance by the Method of Moments, considering the collision efficiency and a better description of breakage, with further coupling with Computational Fluid Dynamics for the hydrodynamics of the slurry, capable of predicting settling (bed formation). Sampaio et al.[10] expanded the population balance solution to the Direct Quadrature Method of Moments[11–13], considering all aforementioned phenomena and yet including the particle temperature alongside with the particle size in a bivariate distribution. Sampaio et al.[10] is the most complete population balance found in the extent of the literature review herein done for systems without oil.

For systems containing oil, only two models exist in the literature. Camargo and Palermo[14,15] modeled the stable agglomerate size (that is, the population balance solved for the steady-state) for a fractal agglomerate geometry considering the competition between adhesion forces and mechanical breakage of the agglomerates induced by flow shear. Colombel et al.[16,17] applied discrete mathematics (the method of classes) to solve the population balance, coupling with agglomeration efficiency due to electrostatic forces[6].

Some further intermediary steps of the agglomeration process were however never considered in the gas hydrates literature. After an efficient collision, the particles remain together on what is called an aggregate. The aggregate may disrupt due to flow shear[18], or consolidate due to the crystallization of both particles into an agglomerate[19,20]. The competition of both phenomena give an expression for the agglomeration efficiency[21–23], that is, the percentage of particles that turns into agglomerates after an efficient collision. In a different approach in literature, the formation of liquid bridge is considered to enhance agglomeration, where the agglomeration efficiency is considered proportional to the percentage of the particle surface covered by the liquid bridge-former fluid, called *binder*[24–27]. As already discussed in part I[1], electrostatic forces are important for the submicron scale, related to water-continuous flow (or systems without oil), which was indeed the application of major part of the agglomeration models developed for gas hydrates up to now[4,7–10]. However, in oil-continuous systems, the particles are close to the mm-scale, and therefore liquid bridge forces are most likely to describe agglomeration. For gas hydrate, the existence of the liquid bridge is related to wet particles, that is, a layer of water furnished by permeation of water through the porous particle that wets its outer surface. Due to the sealing-up of capillaries with time, a particle that was initially wet can dry out, therefore changing the agglomeration efficiency. The approach herein adopted is that flow shear competes with capillary forces due to the existence of the liquid bridge when the particles are wet, leading to an expression for the disruption rate. This couples the two opposing ways of modeling agglomeration efficiency in literature, namely consolidation vs disruption rates[18–23] and liquid bridge formation[24–27].

Furthermore, a constant topic of the more advanced agglomeration models[7,8,14–17] is the coupling with apparent viscosity correlations[28,29], where the viscosification because of hydrate formation is related to plugging of pipelines when the head loss exceeds the pumping power of the system. This is not incorrect, but: (i) the apparent viscosity models/correlations are often valid for small, non-interacting particles in dilute systems[30–37], and (ii) systems that present large agglomerates will plug

much faster due to the accumulation/jamming of these agglomerates, causing partial restrictions that substantially increase pressure drop in a flow line[38,39]. That is, a criterion to understand if the system will be dispersed after the onset of hydrate formation is required to assure the coupling with apparent viscosity models/correlations.

In this article, the evolution of a wet particle that dries out with time is modeled and introduced into the determination of the disruption rate (and thus the agglomeration efficiency), and afterwards coupled into a population balance solved through the Method of Moments. The model simplification leads to simple expressions for the time the particle takes to dry out, the agglomerate size evolution in time, and the stable agglomerate size. Finally, we propose a criterion to classify whether agglomeration is important or not, that is, if the system will remain dispersed or if large agglomerates will form after the onset of hydrate formation, in means of the subcooling of the system and the interfacial properties (use of additives).

## 2. Mathematical model

The purpose of the agglomeration model is to predict the evolution of the particle/agglomerate size in time. The mathematics that describe agglomeration is called *Population Balance*[40,41], which consists of a Partial Differential Equation (PDE) where the parameter to be solved is the Particle Size Distribution (PSD), given by $f\left(L,t\right)$, where $L$ is the particle size and $t$ is time. This distribution is shown in Figure 1. Several mathematical approaches exist to solve the PDE. The one adopted here is the Method of Moments, which consists into integrating the particle size distribution weighted by the particle size to the $j^{th}$ order. The *moment of the particle size distribution of $j^{th}$ order* is defined as

$$M_j = \int_0^\infty f L^j dL \tag{1}$$

Therefore, the PDE is transformed into a systems of Ordinary Differential Equations (ODEs) of size $j \times j$. Infinite moments exist, but here we are interest from the $0^{th}$ to the $3^{rd}$ moment because of their physical meaning: (i) the moment of $0^{th}$ order represents the number of particles by unit volume of liquid $\forall_L$, given in $\left[\text{particles}/\text{m}^3\right] \approx \left[\text{m}^{-3}\right]$; (ii) the moment of $1^{st}$ order represents the sum of the length of the particles per unit volume $\left[\text{particles} \cdot \text{m}/\text{m}^3\right] \approx \left[\text{m}^{-2}\right]$; (iii) the moment of $2^{nd}$ order is proportional (by a shape factor $\phi_2$) to the total interfacial surface between the particles

and the continuous liquid phase per unit volume $\left[\text{particles}\cdot\text{m}^2/\text{m}^3\right]\approx\left[\text{m}^{-1}\right]$; and (iv) the moment of 3rd order is proportional (by a volume factor $\phi_3$) to the total volume of the particles per unit volume $\left[\text{particles}\cdot\text{m}^3/\text{m}^3\right]\approx\left[-\right]$. Based on these definitions, the number of particles in the system $n_p$, the average particle radius $r_p$, the average outer surface of the particle $A_{out}$, and the average volume of the particle $\forall_p$, are related to the moments as

$$n_p = M_0 \forall_L \tag{2}$$

$$r_p = \frac{M_1}{M_0} \tag{3}$$

$$A_{out} = \phi_2 \frac{M_2}{M_0} \approx 4\pi \frac{M_2}{M_0} \tag{4}$$

$$\forall_p = \phi_3 \frac{M_3}{M_0} \approx \frac{4\pi}{3} \frac{M_3}{M_0} \tag{5}$$

where $\phi_2 = 4\pi$ and $\phi_3 = 4\pi/3$ are the shape and volume factors for spherical particles when considering the particle radius $r_p$ as the characteristic length $L$ of the particle. That is, by the solution of a $4\times4$ ODE system for $M_0 - M_3$, we are able to retrieve the evolution of the average parameters of the particle size distribution, especially the particle/agglomerate radius, which is the main interest here. The outer surface is also important to estimate the particle/bulk interface, that plays a role in the mass transfer system for growth kinetics (part II[2]). The particle/agglomerate volume (or its volumetric fraction) will further be important to estimate the apparent viscosity of the hydrate-oil slurry, which will be of interest in the future parts of this series once hydrate formation is coupled to multiphase flow.

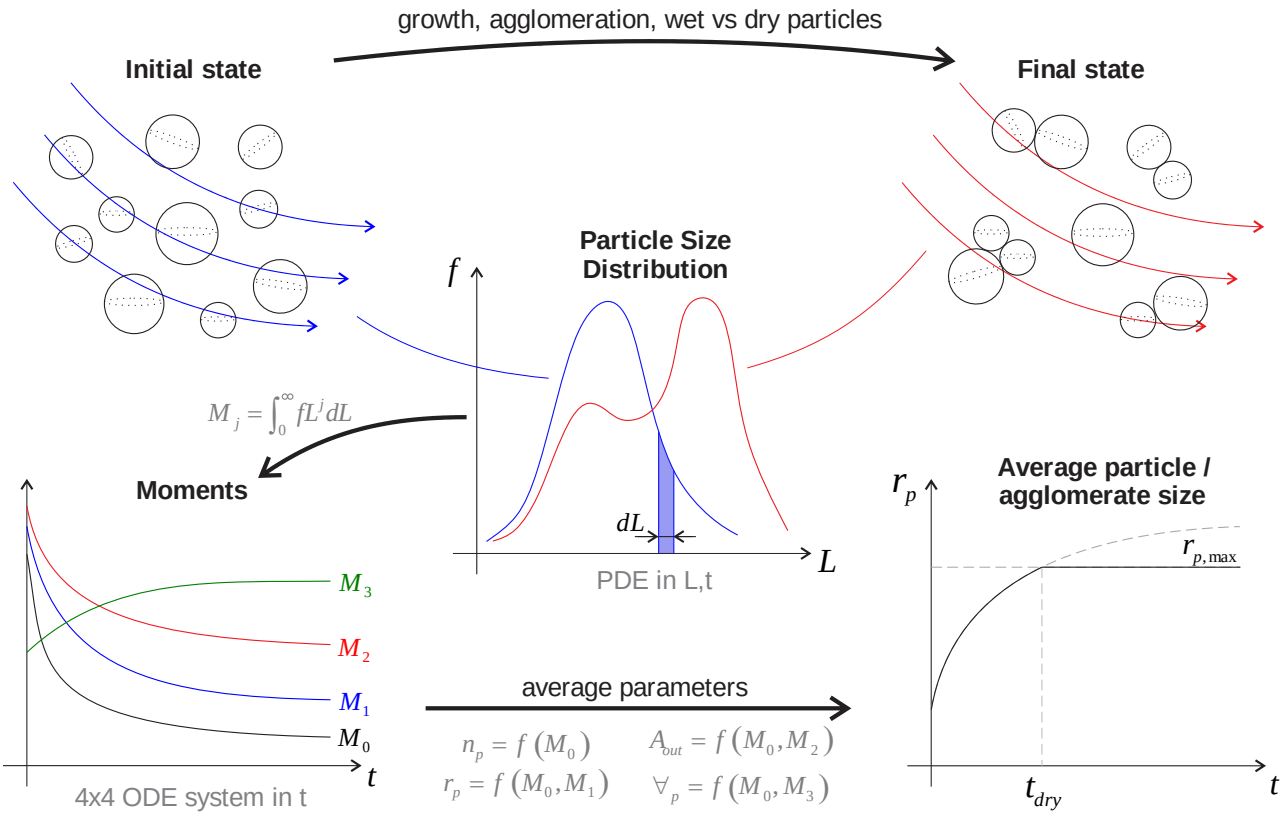


Figure 1. Representation of the mathematic approach adopted to solve the population balance. The particle population is represented by a particle size distribution, which is integrated to find the moments, that afterwards give the average parameters evolution in time, such as the number of particles $(n_p)$, the average particle/agglomerate size $(r_p)$, its outer surface $(A_{out})$, and its volume $(\forall_p)$.

The population balance, written in the Method of Moments up to the 3rd order, considering growth and agglomeration processes, and neglecting breakage (since it is difficult to determine how many pieces the particle will split into, and their relative sizes[4]), is (see demonstration #1 of the Supporting Information)

$$\begin{cases} \dfrac{dM_0}{dt} = -\dfrac{K_{agg}}{2} M_0^2 \\ \dfrac{dM_1}{dt} = GM_0 + K_1 K_{agg} M_1 M_0 \\ \dfrac{dM_2}{dt} = 2GM_1 + K_2 K_{agg} M_2 M_0 \\ \dfrac{dM_3}{dt} = 3GM_2 \end{cases} \tag{6}$$

where $K_{agg}$ is the kernel of agglomeration (which modeling is the focus of this article), $K_1, K_2$ are called agglomerate shape coefficients (see demonstration #2 of the Supporting Information for a geometrical model in order to determine these coefficients), and $G = \dfrac{dr_p}{dt}$ is the linear outer growth rate of the particle, derived from the growth kinetic model, eq (S12) of the Supporting Information of part II[2], repeated below

$$G = \frac{M_0}{M_2} \frac{(\eta+1)}{(1-\varepsilon)} \frac{M_h}{\rho_h} \min\left\{ \begin{array}{l} \zeta \dfrac{\pi}{3} \dfrac{\rho_w}{\eta M_w} \dfrac{r_c}{\tau^2} \dfrac{\sigma_{o/w} \cos\theta_{o/w/h}}{\mu_w} \dfrac{M_2}{M_1} \varepsilon \; ; \\ \dfrac{k_i}{H_o} \dfrac{M_2}{M_0} \left[ C_b - H_o f_{eq} - \dfrac{M_0}{M_2} \dfrac{1}{h_{m,p/b}} \left( -\dfrac{dn_{g,i}}{dt}\bigg|_{hyd} \right) \right] \end{array} \right\} \tag{7}$$

where the average particle size and the average outer surface were written in terms of the moments as $r_p \approx \dfrac{M_1}{M_0}$ and $4\pi r_p^2 \approx \dfrac{M_2}{M_0}$. Notice that the shape and volume factors are neglected $\phi_2 = \phi_3 = 1$, since the agglomerates are not necessarily spherical, as the particles of part II[2]. The geometrical sense is given by the agglomerate shape coefficients $K_1, K_2$ when dealing with the particle population. The meaning of the parameters in eq (7) is referred to the nomenclature section and the physics description to part II[2]. It is important to notice, nevertheless, that the minimum function describes the competition between water permeation through the porous particle (first term) and crystal integration in the outer surface (second term), and this is the basis for further modeling the agglomeration efficiency and the time the particles takes to dry out.

Eqs (6) are solved with a 4th order Runge-Kutta Method. Nucleation is considered to be *instantaneous*[42], that is, when nucleation of the first particles is initiated (at $t = 0$), a number of particles $n_{p,in}$ nucleates with an average radius $r_{p,in}$, and no further nucleation occur for $t > 0$. The

nucleation is therefore the initial condition for the population balance, and the name "onset of formation" is preferred, since no modeling of the nucleation itself is made in this article (notice that nucleation modeling requires molecular size-scales[43,44]). By the experimental evidence that the porous particles instantly trap water during the onset of formation (discussed in part I[1]; experimental observations of Melchuna et al.[45] and Kakitani et al.[46,47]), then the number of particles relates to the initial particle radius as

$$n_{p,in} = \frac{3}{4}\frac{\mathrm{WC}\forall_L}{\pi r_{p,in}^3} \tag{8}$$

where $\mathrm{WC}$ is the water cut and $\forall_L$ is the volume of liquid (water + oil). Here, the initial particle size comes from visualization of the experiment, but for further model application, it is fair to consider that the particles will have an initial size in the order of magnitude of the water droplet size prior to the onset of hydrate formation, given enough flow shear in order to avoid stratification of the phases during the onset. Several models for the droplet size $r_d$ exist[48–51], usually following the shape of $r_d \propto \mathrm{We}^b\,\mathrm{Re}^c$, where $\mathrm{We}$ and $\mathrm{Re}$ are the Weber and Reynolds numbers of the liquid continuous phase, respectively.

Finally, from eq (2) and by using the relation between moments $M_j = \phi_j M_0 r_{p,in}$ for $t = 0$, with $\phi_1 = 1$, $\phi_2 = 4\pi$ and $\phi_3 = 4\pi/3$ the geometric factors for initially spherical particles, the initial condition of the population balance of eqs (6) becomes

$$\begin{cases} M_0\big|_{t=0} = \dfrac{3}{4}\dfrac{\mathrm{WC}}{\pi r_{p,in}^3} \\ M_1\big|_{t=0} = \dfrac{3}{4}\dfrac{\mathrm{WC}}{\pi r_{p,in}^2} \\ M_2\big|_{t=0} = 3\dfrac{\mathrm{WC}}{r_{p,in}} \\ M_3\big|_{t=0} = \mathrm{WC} \end{cases} \tag{9}$$

***Developing an Expression for the Kernel of Agglomeration***

Figure 2 depicts the steps of agglomeration. Two particles need to efficiently collide in order to form an aggregate. If the surface of the particle is wet, that is, water is furnished to the outer surface by permeation through the porous medium, then a liquid bridge forms, holding the aggregate

together. The aggregate can either disrupt because of flow shear, or consolidate (crystallization of the liquid bridge into a crystal bridge, 'welding' both particles), forming an agglomerate. The agglomerate is much more stable than the aggregate, since the force holding the agglomerate together is due to the yield stress of the solid crystal, whereas the force holding the aggregate together is given by the oil-water interfacial tension. In this model, we consider that once aggregates consolidate, there is not disruption anymore (hypothesis of no breakage). As well, as porosity of the particle decreases with time (see part II[2]), the particle stops furnishing water to its outer surface, and the particle eventually dries out after a time scale $t_{dry}$. Dry particles do not form liquid bridges anymore, and therefore we consider that the agglomeration process stops, reaching a stable (maximum) agglomerate radius $r_{p,\max}$.

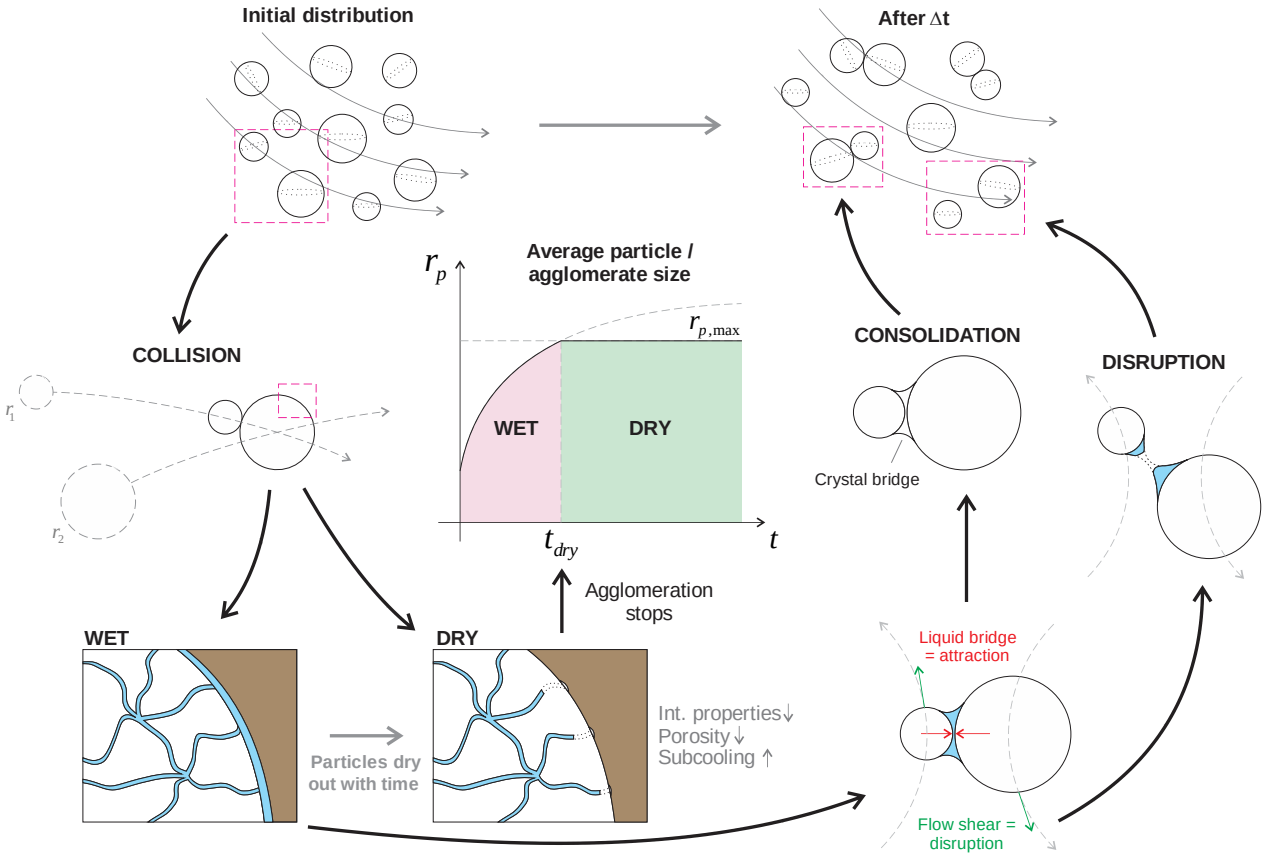


Figure 2. The final result sought in the model is the average particle/agglomerate size evolution in time. In order for two particles to agglomerate, they need to efficiently collide. If the particle is wet, the binding forces because of the liquid bridge compete with disruption forces because of flow shear. An agglomerate forms if the particles remain aggregated for enough time for the liquid

bridge to consolidate into a crystal bridge. With time, the particles dry out because of porosity decrease, thus the liquid bridges do not form anymore, and agglomeration stops, reaching a stable agglomerate size.

The kernel of agglomeration is given by[52]

$$K_{agg} = k_{col}\eta_{col}\eta_{agg} \tag{10}$$

where $k_{col}$ is the collision rate, $\eta_{col}$ is the collision efficiency, and $\eta_{agg}$ is the agglomeration efficiency. The expression for the collision probability of shear-induced flow of Smoluchowski[5] is adopted

$$k_{col} = \frac{4}{3}\dot{\gamma}\left(r_1 + r_2\right)^3 \approx \frac{32}{3}\dot{\gamma}\left(\frac{M_1}{M_0}\right)^3 \tag{11}$$

where the colliding particles are considered to have the same radius, $r_1 = r_2 = r_p \approx \frac{M_1}{M_0}$. This expression holds for a constant shear rate, but is herein extrapolated for turbulent regime by considering an average shear rate. Further discussion on Smoluchowski's[5] relation and its applicability in this study is given in demonstration #3 of the Supporting Information.

The collision efficiency is neglected, that is, $\eta_{col} \approx 1$, since the available models depend on the interparticle distance, and therefore incur in Lagrangian tracking of each particle, which increases considerably the complexity of the problem. If ever the Lagrangian tracking of the particles is considered, then extra forces due to the inertia of the liquid drained in between particles[53] and the impulse forces after collision can be considered[54]. The collision efficiency can be further related to the energy potential between particles, that is, to electrostatic forces when dealing with submicron-scale particles[55], or to the energy necessary to disrupt the water layer around the wet particle in order to form the liquid bridge when dealing with particles in the mm-scale. This is not considered here.

Figure 3 depicts a simplified scheme of the agglomeration steps defined in Figure 2. From this scheme, the agglomeration efficiency comes from the competition between the disruption and consolidation rates[21,23,52]

$$\eta_{agg} = \left(1 + \frac{k_d}{k_c}\right)^{-1} \tag{12}$$

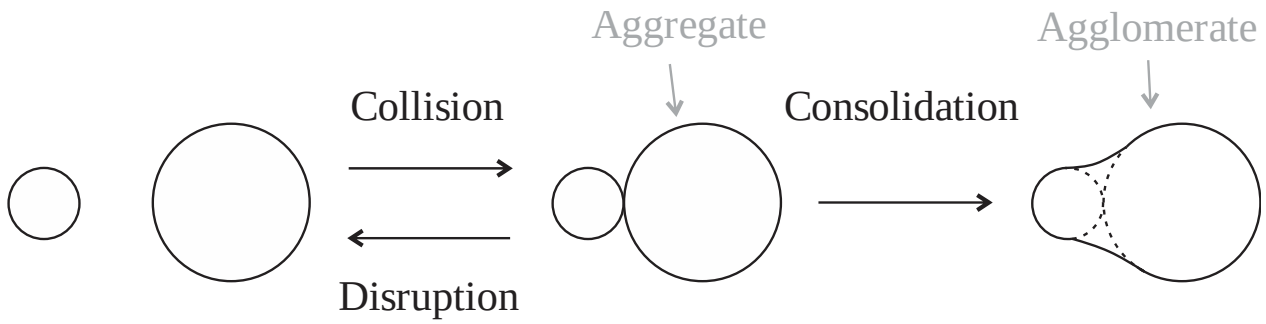


Figure 3. Simplified scheme of the agglomeration steps.

The consolidation rate $k_c$ follows the approach of David et al.[18], but further highlights some extra parameters of the crystal such as its porosity and the ratios of density and molar mass between hydrate and water. The consolidation rate is the inverse of the time required to crystallize the water volume contained in the liquid bridge between the particles[21], $k_c = 1/t_c$, as shown in Figure 4a. The volumetric consumption of water due to crystallization $-d\forall_w/dt$ can be linearly approximated to the ratio of the liquid bridge volume and the time required for consolidation, $\forall_b/t_c$, where index $b$ stands for "(liquid/capillary) bridge" and index $c$ for "consolidation". The water volumetric consumption rate is related to the hydrate volumetric formation rate by using the "stoichiometric" relation $1G + \eta H_2O \rightarrow (\eta+1)Hyd$, where $\eta$ is the hydration number, which gives $-\frac{d\forall_w}{dt} = \frac{\eta+1}{\eta}\frac{M_h}{M_w}\frac{\rho_w}{(1-\varepsilon)\rho_h}\frac{d\forall_h}{dt}$. In this expression, $(1-\varepsilon)\rho_h$ represents the density of the porous hydrate (without water entrapped in the capillaries), and $\rho_h$ is the density of a perfect hydrate crystal (density of the solid matrix of the porous medium). Finally, the hydrate volumetric formation rate is related to the linear outer growth rate $G$ of eq (7) through $\frac{d\forall_h}{dt} = 2GA_b$, where $A_b$ is the particle surface covered by the liquid bridge (the crystalizing surface), and the multiplication by 2 comes from the fact that both particles are crystallizing at velocity $G$. From all of these considerations, the consolidation rate becomes

$$k_c = 2\frac{\eta+1}{\eta}\frac{M_h}{M_w}\frac{\rho_w}{(1-\varepsilon)\rho_h}\frac{A_b}{\forall_b}G \tag{13}$$

The particle surface covered by the liquid bridge $A_b$ is the surface of a spherical cap with polar angle $\varphi_b$ wetted by the liquid bridge, as presented in Figure 4b

$$A_b = 2\pi r_p^2 \left(1-\cos\varphi_b\right) \approx \frac{1}{2}\frac{M_2}{M_0}\left(1-\cos\varphi_b\right) \tag{14}$$

where the particle outer surface is related to the moments by $\frac{M_2}{M_0} \approx 4\pi r_p^2$. The volume of the liquid bridge is approximated by a cylinder of base $\pi\left(r_p \sin\varphi_b\right)^2$ and height $2r_p\left(1-\cos\varphi_b\right)$, minus the two spherical cap volumes, each one with volume $\forall_{cap} = \frac{\pi}{3} r_p^3 \left(2+\cos\varphi_b\right)\left(1-\cos\varphi_b\right)^2$, as presented in Figure 4c. Therefore

$$\underset{\frac{3}{2}\frac{M_3}{M_0}}{\forall_b} = 2\pi r_p^3 \left(1-\cos\varphi_b\right)\left[\left(\sin\varphi_b\right)^2 - \frac{1}{3}\left(2+\cos\varphi_b\right)\left(1-\cos\varphi_b\right)\right] \tag{15}$$

where the particle volume is related to the moments by $\frac{M_3}{M_0} \approx \frac{4}{3}\pi r_p^3$. Notice that the particles are considered to touch each other and to have the same radius $r_p$, and that the oil-water-hydrate wetted angle, which curves the surface of the liquid bridge (Figure 4c), is neglected for the sake of simplification. Using eqs (14) and (15)

$$\frac{A_b}{\forall_b} \approx g_1 \frac{M_2}{M_3} \tag{16}$$

$$g_1 = \frac{1}{3}\left[\left(\sin\varphi_b\right)^2 - \frac{1}{3}\left(2+\cos\varphi_b\right)\left(1-\cos\varphi_b\right)\right]^{-1} \tag{17}$$

where the geometric factor $g_1$ depends on the polar angle covered by the liquid bridge $\varphi_b$, which is unknown a priori. It is plausible to say, nevertheless, that is lays in the range of $30^o \le \varphi_b \le 60^o$, giving values in the order of $1 \le g_1 \le 2.7$. Using eq (16) in (13), the consolidation rate becomes

$$k_c = g_2 \frac{G}{(1-\varepsilon)}\frac{M_2}{M_3} \tag{18}$$

$$g_2 = 2g_1 \frac{\eta+1}{\eta}\frac{M_h}{M_w}\frac{\rho_w}{\rho_h} \tag{19}$$

where $g_2$ is a factor that considers the liquid bridge geometry (from $g_1$) and the ratio of water to hydrate properties, and lays in the range of $2.4 \le g_2 \le 6.8$ when considering the values of Table 1. It is important to notice that, in the approach herein adopted (Method of Moments), there is no distinction between the sizes of the particles that form the agglomerate. Therefore, the average representations of the total surface of particles per unit volume of liquid $(M_2)$ and of the total volume of particle per unit volume of liquid $(M_3)$ are used. If a discrete mathematics approach that tracks the size of the aggregating particles is employed, then the consolidation rate can be used in terms of the particle radius. The liquid bridge will then relates to the smaller particle that forms the aggregate, thus $r_p = \min(r_1, r_2)$ shall be adopted, where $r_1, r_2$ stand for the radii of the aggregating particles.

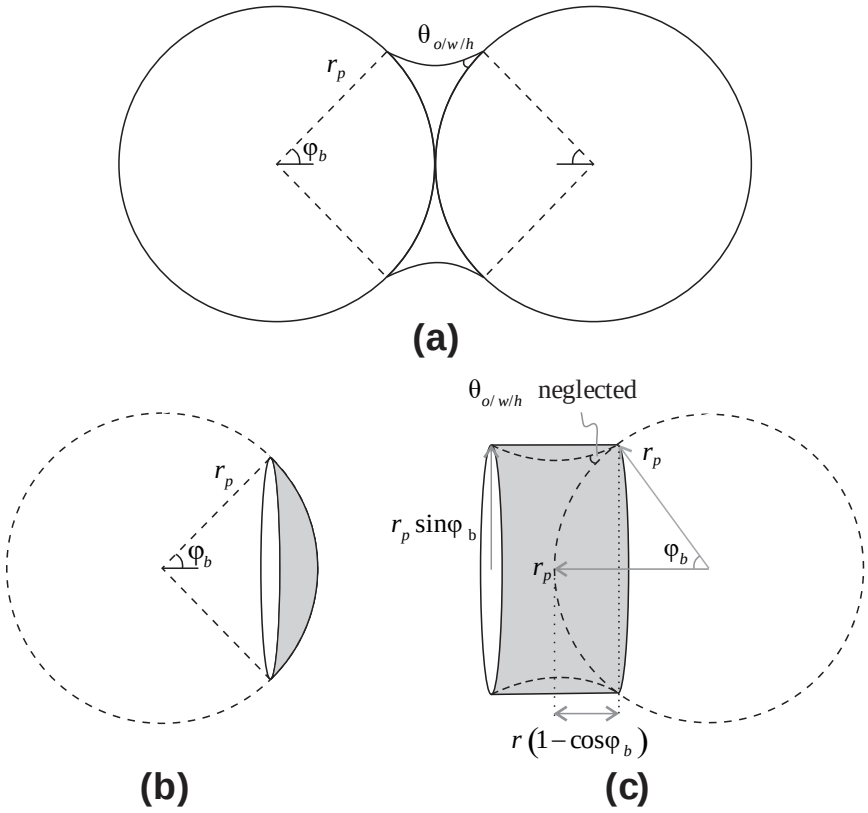


Figure 4. (a) Aggregate united by liquid bridge. (b) Spherical cap described by the polar angle $\varphi_b$ wetted by the liquid bridge. (c) Liquid bridge volume described by a cylinder minus two spherical caps.

To model the disruption rate, an energy approach similar to the one used to estimate droplet size[48,51] is adopted. When two wet particles of identic radius $r_p$ aggregate, the oil-water interface decreases due to the formation of the liquid bridge from a state described by two spherical caps, where $A_{disaggregated} \approx 4\pi r_p^2 \left(1-\cos\varphi_b\right)$ (Figure 4b), to a state due to the cylinder surface, $A_{aggregated} \approx 4\pi r_p^2 \left(1-\cos\varphi_b\right)\sin\varphi_b$ (Figure 4c). Therefore, the increase of interfacial energy per unit time is the disruption rate $k_d$, in [$s^{-1}$], multiplied by the surface variation from the aggregated to the disaggregated state, multiplied by the oil-water interfacial tension $\sigma_{o/w}$

$$\Delta\dot{E}_{\text{int}} = k_d \sigma_{o/w} \Delta A \approx g_3 k_d \sigma_{o/w} \frac{M_2}{M_0} \tag{20}$$

$$g_3 = \left(1-\cos\varphi_b\right)\left(1-\sin\varphi_b\right) \tag{21}$$

where the particle outer surface is related to the moments by $\frac{M_2}{M_0} \approx 4\pi r_p^2$. The geometric factor $g_3$ lays in the range $6.7\times10^{-2} \le g_3 \le 8.6\times10^{-2}$ when $30^o \le \varphi_b \le 60^o$. Again, the representation using the particle radius and considering $r_p = \min\left(r_1, r_2\right)$ shall be adopted when the size of the radii of the aggregating particles $r_1, r_2$ is known. The energy per unit time and per unit mass furnished by the flow is called the energy dissipation rate $\varepsilon_t$, where $\varepsilon_t \propto \frac{\mu_o}{\rho_o}\dot{\gamma}^2$ from Kolmogorov theory, but equality is considered since the expression developed is as well only a proportionality. The absolute energy per unit time furnished by a mass of liquid $m_L$ to each aggregate (if all particles are aggregated, then the number of aggregates would be $n_p/2$) is then proportional to

$$\Delta\dot{E}_{flow} \propto \frac{2m_L\varepsilon_t}{n_p} \approx \frac{2\mu_o\dot{\gamma}^2}{M_0} \tag{22}$$

where $\mu_o$ is the dynamic viscosity of the oil continuous phase. Notice that this expression is independent of the liquid volume, since it is canceled out by recognizing that $\frac{m_L}{n_p} = \frac{\rho_L \forall_L}{M_0 \forall_L} = \frac{\rho_L}{M_0}$.

By an energy balance, the increase in energy due to the disruption of the aggregates is proportional to the energy furnished by the flow, $\Delta\dot{E}_{\text{int}} \propto \Delta\dot{E}_{flow}$, and therefore from eqs (20) and (22), the disruption rate comes

$$k_d = \frac{2}{g_3}\frac{\mu_o \dot{\gamma}^2}{\sigma_{o/w} M_2} \tag{23}$$

Eqs (18) and (23) are therefore introduced in eq (12) to find the agglomeration efficiency

$$\eta_{agg} = \left[1 + g_4 \frac{(1-\varepsilon)\,\mu_o \dot{\gamma}^2}{G\sigma_{o/w}} \frac{M_3}{M_2^2}\right]^{-1} \tag{24}$$

$$g_4 = \frac{2}{g_2 g_3} = \left(\frac{\eta}{\eta+1}\frac{M_w}{M_h}\frac{\rho_h}{\rho_w}\right)\left[\frac{3(\sin\varphi_b)^2 - (2+\cos\varphi_b)(1-\cos\varphi_b)}{(1-\cos\varphi_b)(1-\sin\varphi_b)}\right] \tag{25}$$

where the factor $g_4$ represents the geometry of the liquid bridge and the hydrate-to-water properties ratio, and lays in a range of $4.4 \le g_4 \le 12.3$ when considering $30^o \le \varphi_b \le 60^o$ and the values of Table 1. Finally by using eqs (11) and (24) in (10), and by neglecting the collision efficiency $(\eta_{col} \approx 1)$, the kernel of agglomeration becomes

$$K_{agg} = \frac{32}{3}\dot{\gamma}\left(\frac{M_1}{M_0}\right)^3 \left[1 + g_4 \frac{(1-\varepsilon)\,\mu_o \dot{\gamma}^2}{G\sigma_{o/w}} \frac{M_3}{M_2^2}\right]^{-1} \tag{26}$$

where $G$ comes from eq (7). This expression for the kernel of agglomeration relates the agglomeration efficiency between two wet hydrate particles that form a liquid bridge of interfacial tension $\sigma_{o/w}$ with (i) the crystal growth velocity $G(\Delta T)$, which depends on the driving force (subcooling) of crystallization, and (ii) the shear rate $\dot{\gamma}$ of the flow, associated to the probability of collision between two particles, and to the disruption rate of aggregates. In eq (43) of part II[2], a criterion for the existence of dry particles was proposed when considering hydrophilic hydrates in oil continuous flow. This criterion for a dry particle is repeated below

$$\frac{1}{12}\left(\frac{\rho_w}{\mu_w M_w}\right)\left(\frac{\zeta r_c}{\tau^2}\right)\frac{(\sigma_{o/w}\cos\theta_{o/w/h})}{\eta k_i (f_g - f_{eq})}\frac{M_0}{M_1}\varepsilon < 1 \tag{27}$$

where $r_p = M_1/M_0$ is used to relate the particle radius with the moments. Because the porosity $\varepsilon$ decreases with time, following eq (32) of part II[2], then an initially wet particle can dry out with time. When the particle becomes dry, the liquid bridge that holds the aggregate together stops existing, that is, there is no interfacial tension between the aggregate and, mathematically, $\sigma_{o/w} \to 0$. In this case, the disruption rate tends to infinite, $k_d \to \infty$ from eq (23), causing the agglomeration efficiency to tend to zero, $\eta_{agg} \to 0$ from eq (12). Therefore, the kernel of agglomeration also tends

to zero, $K_{agg} \to 0$ from eq (10), and the system stops agglomerating once the particles become dry. That is, the criterion of eq (27) predicts that, at some point, the system stops agglomerating. This trend is abrupt since all water is considered to vanish from the outer surface of the particle at the same time, whereby it will most probably gradually vanish. As discussed by Balakin et al.[27], the ratio of surface covered by the liquid bridge-former fluid (*binder*) is related to an extra term of probability to form the agglomerates. If this is ever considered in criterion of eq (27), it would soften the abrupt stop of the agglomeration. This is however not considered in this study in order to avoid any extra parameter fitting.

A further mechanism that can still be put in question is the fact that, upon collision between particle-particle or particle-wall, the particles are deformed and some water is squeezed from the porous medium, making it available to form the liquid bridge. Furthermore, the flow shear stresses distribution (known as *stresslet* over the particle[36]) can cause the same effect. These two mechanisms are not considered in the modeling of the criterion of eq (27). This modeling would imply in tracking the particles and in predicting their deformation, which implies in much greater detail of the flow and its interaction with the solid structures, which is beyond the purpose of this study.

Finally, it is important to state that the agglomeration model is coupled to the growth kinetic model of part II[2], which estimates the amount of gas consumed and the porosity decrease in time. However, the model of part II[2] was developed for non-agglomerating systems, where the number of particles $n_p$ and the average particle radius $r_p$ remains constant along the entire simulation. When the system agglomerates, the moments of the particle size distribution need to be used instead of the number, length and surface of the particles. The necessary modifications are shown in demonstration #4 of the Supporting Information.

## 3. Model Closure and Comparison with Experimental Data

The model is regressed and compared to the experimental dataset of Kakitani et al.[46,47]. The characteristics of the apparatus are given in Table 2 and the grid test is given in Table 3. Several windows are placed along the rock-flow cell. Some selected photos were treated manually in order to extract an average particle size and its evolution in time so as to compare with the agglomeration model. The correct way to do so would be by the use of an instrumentation capable of measuring

the Particle Size Distribution $f(L,t)$, which however is an open issue in hydrates research for large particles and dense systems. Notice that the commonly adopted instrumentation is the FBRM (Focus Beam Reflectance Measurement), which gives a measure of the chord length distribution, not particle size, and has 1-1000 μm range of measurement, far smaller than the particles/agglomerates treated in this study. The method adopted (manual treatment of images), although not precise, is able to identify, at least, the order of magnitude of the average particle/agglomerate size with time.

Table 1 presents the closure values adopted. As already discussed in part II[2], complete closure of such model is hard to achieve, and here *we stick to the evaluation of the orders of magnitude of both input and output parameters, and the trends that the model is able to capture*. Closure for micro-scale parameters of the crystal integration process (the constant of proportionality $k_i$) and of the porous medium (initial porosity $\varepsilon_{in}$, capillary radius $r_c$, tortuosity $\tau$, and interconnectivity $\zeta$) are yet scarce in literature. These were considered the same as in part II[2], but the initial porosity, herein adopted to be 90% instead of 60%, leading to longer times for the particle to turn dry in order to fit the experimental data of the particle size evolution in time. The porous medium interconnectivity was considered to depend on the subcooling, where the maximum limiting value of 0.02 was used for the cases of 7.5 K subcooling, and the minimum value of 0.001 for the cases of 18 K subcooling (see Table 1 of part II[2]).

The agglomeration model introduces new closure values regarding the flow of the continuous phase. The oil viscosity is hard to accurately determine at 70 bar, and a value of ~10 cP is considered to represent the order of magnitude of it, although the gas concentration evolves in time because of the competition between gas absorption and bulk depletion when hydrates form (non-equilibrium problem). The oil viscosity affects the estimation of the shear rate, which depends on flow turbulence. From CFD simulations of air-water in a rock-flow cell of similar geometry, the shear rate is estimated to be in the order of 1 to 10 $s^{-1}$ in the liquid bulk. Herein, the shear rate is considered to be in the order of magnitude of a turbulent, single-phase, developed, steady-state flow in smooth pipes (see demonstration #5 of the Supporting Information). The average fluid velocity inside the rock-flow cell is unknown, but should remain inside the velocity-scale $U \propto 2\omega L$, being $\omega$ the oscillation rate of the rock-flow cell, and $L$ the rock-flow cell length.

Finally, there are some intrinsic parameters of the model that need regression. For the kinetic model, there are two parameters, $\lambda, \alpha_p$. The first one is the birth-to-death ratio of capillaries, where $1-\lambda = 0.8\times10^{-2}$ was regressed, instead of $1-\lambda = 1.9\times10^{-2}$ for the experimental case of part II[2]. The second parameter is called efficiency of particles interacting with the bulk $\alpha_p$, which depends on the gas spatial distribution inside the continuous phase (not modeled, since a bulk is considered, that is, the same concentration is supplied to every particle). This parameter depends on the system agitation, on the distance of the particles to the gas-oil interface, and on the flow being dense or dilute. In part II[2], $\alpha_p \approx 0.03$ was regressed because the system is very large and gas absorption occurs in a restricted area. Herein, for the rock-flow cell, $\alpha_p \approx 0.15$ for the 7.5 K subcooling cases, which is one order of magnitude higher due to the use of a smaller system, but still small because the system agitation is low (rock-flow cell is a gravity-induced flow). For the cases of 18 K subcooling, the regressed value was $\alpha_p \approx 0.06$, explained by a higher competition of gas consumption between particles when the driving force is higher. The intrinsic parameters of the agglomeration model are the agglomerate shape coefficients, where Herri et al.[4] values are adopted, $K_1 = -0.262$ and $K_2 = -0.113$, and the proportionality factor between consolidation and disruption rates, where $g_4 = 9$ is adopted as being a central value in the range of the geometrical model considered, eq (25).

Figure 5 presents comparison of the model with experimental data for the average gas consumption rate $(n_g/t)$ and the average particle increase rate $[(r_p - r_{p,in})/t]$, evaluated at time instants 20 min, 40 min, 1 h, 2 h, 3 h, and 4 h after the onset of formation. For instance, neglect the circles of Figure 5, which represent the simplified model to be introduced in section 5. The model presents deviations inside the range of ±40%, that is, it is able to capture the order of magnitude of both gas consumption (in the order of 0.15 to 0.25 mols of gas after 4 h for the 0.5 L of liquid at 10% water cut) and the order of magnitude of the agglomeration rate (to be discussed in the next section). The model overpredicts considerably the gas consumption rate when bed formation occurs (case #2 of Figure 5, in red, also to be discussed in the next section). The simulations were held using a time step of 3 s, where smaller time steps do not present considerable improvement of the results. Convergence of this fairly large time step shows the robustness of the 4$^{th}$ order Runge-Kutta Method for this problem.

Table 1. Closure values for model evaluation[a].

| Parameter | Adopted value |
|---|---|
| Constant of proportionality of crystal integration[2] | $k_i \approx 4.1\times10^{-11}$ mol/(m$^2$sPa) |
| Absorption coefficient[2] | $\frac{k_{abs}A_{g/b}}{\forall_b} \approx 1\times10^{-2}$ s$^{-1}$ |
| Mass transfer coefficient between particle and bulk[56b] | $h_{m,p/b} = \frac{\mathrm{Sh_p} D_{g/o}}{2r_p}$ with $\mathrm{Sh_p} = 2 + 0.6\,\mathrm{Re_p^{1/2}}\,\mathrm{Sc^{1/3}}$, giving $1.9\times10^{-4} \le h_{m,p/b} \le 2.6\times10^{-4}$ m/s |
| Henry's constant of gas in water[57] and in oil[2c] | $H_{\mathrm{CH4}/w} = 2.2\times10^{-5}$ mol/(m$^3$Pa) (at 2$^o$C)<br>$H_{mix/w} = 2.2\times10^{-5}$ mol/(m$^3$Pa) (at 2$^o$C)<br>$H_{mix/w} = 1.8\times10^{-5}$ mol/(m$^3$Pa) (at 12.5$^o$C)<br>$H_o \approx 2.7\times10^{-4}$ mol/(m$^3$Pa) (order of magnitude for any hydrocarbon gas in oil) |
| Water, methane, and gas mixture properties | Evaluated through RefProp[58] |
| Oil properties[1,47d] | $\rho_o = 850\,\mathrm{kg/m^3}$ ; $\mu_o \approx 10\times10^{-3}$ Pa.s ; $\sigma_o \approx 0.0257$ N/m |
| Hydrate properties[e] | $CH_4$ hydrates (sI structure)<br>$\rho_h = 918.1\,\mathrm{kg/m^3}$ ; $M_h = 17.7\times10^{-3}$ kg/mol<br>Gas mixture hydrate (sII structure)<br>$\rho_h = 969.1\,\mathrm{kg/m^3}$ ; $M_h = 18.05\times10^{-3}$ kg/mol<br>For both structures, the hydration number is considered $\eta \approx 6$ |
| Diffusivity of gas in water[59,60f] | $D_{\mathrm{CH4}/w} = 1.24\times10^{-9}$ m$^2$/s<br>$D_{mix/w} = 8.06\times10^{-10}$ m$^2$/s |
| Gas fugacity in free phase evaluated at system pressure and temperature $(P,T)$[58g] | $f_{g,\mathrm{CH4}} = 59.7\times10^5$ Pa (at 2 K, 70 bar)<br>$f_{g,\mathrm{mixture}} = 51.0\times10^5$ Pa (at 2 K, 70 bar)<br>$f_{g,\mathrm{mixture}} = 52.1\times10^5$ Pa (at 12.5 K, 70 bar) |
| Gas fugacity at three-phase gas-water-hydrate equilibrium, evaluated at equilibrium pressure related to the system temperature $(P_{eq},T)$[h] | $f_{eq,\mathrm{CH4}} = 29.5\times10^5$ Pa (7.5 K subcooling)<br>$f_{eq,\mathrm{mixture}} = 19.6\times10^5$ Pa (7.5 K subcooling)<br>$f_{eq,\mathrm{mixture}} = 5.7\times10^5$ Pa (18 K subcooling) |
| Driving force | $f_g - f_{eq} = 30.2\times10^5$ Pa (methane, 7.5 K subcooling)<br>$f_g - f_{eq} = 32.5\times10^5$ Pa (gas mixture, 7.5 K subcooling)<br>$f_g - f_{eq} = 45.3\times10^5$ Pa (gas mixture, 18 K subcooling) |
| Initial porosity of particles | $\varepsilon_{in} = 90\%$ |
| Capillary radius[2] | $r_c = 0.5\,\mu\mathrm{m}$ |
| Capillary tortuosity[2,61–63] | $\tau = 5$ |
| Capillary interconnectivity[2] | $\zeta = 0.02$ (7.5 K subcooling) |

| | |
|---|---|
| | $\zeta = 0.001$ (18 K subcooling) |
| Oil-water interfacial tension[i] | $\sigma_{w/o} = 4.97\times10^{-2}$ N/m (without additive) |
| | $\sigma_{w/o+additive} = 3.73\times10^{-2}$ N/m (with additive) |
| Oil-water-hydrate wetted angle (water side) | $\theta_{o/w/h} = 60^{o}$ |
| Birth-to-death ratio of capillaries (regressed) | $1-\lambda = 8\times10^{-3}$ |
| Efficiency of particles interacting with the bulk (regressed) | $\alpha_p = 0.15$ (7.5 K subcooling) |
| | $\alpha_p = 0.06$ (18 K subcooling) |
| Agglomeration model geometrical parameter | $g_4 = 9$ |
| Agglomerate shape coefficients[4] | $K_1 = -0.262$ ; $K_2 = -0.113$ |

Notes: [a] See as well Table 1 of part II[2]. [b] With $\mathrm{Re_p} = 2\rho_o U_{p/b} r_p / \mu_o$ and $\mathrm{Sc} = \mu_o/(\rho_o D_o)$, and considering that the slip velocity is the same velocity of the fluid and that this velocity comes from the velocity scale inside the rock-flow cell, $U_{p/b} \approx 2\omega L$. The diffusivity of gas in oil is considered to be one order of magnitude higher than the one in water, $D_o \approx 10 D_w$. Notice that this procedure, although approximated, does not have significant sensitivity in the results because hydrocarbon gases are much more soluble in oil than in water, and therefore the particle-bulk mass transfer resistance is negligible. [c] Henry's constant of the mixture inside water is adopted as being Henry's constant of methane inside water, since methane presents lower solubility than propane and thus limits crystallization. The reference value of part II[2] for Henry's constant in oil is adopted for both methane and gas mixture. The order of magnitude for oil is representative of any hydrocarbon gas dissolved in any oil. [d] Reference value of part II[2] for the oil surface tension. [e] Density of the solid matrix of hydrates, coming from MultiFlash™[64]. The molar mass comes from the relation $M_h = (M_g + \eta M_w)/(\eta+1)$. [f] For the gas mixture, it is considered that the component with smaller diffusivity in water (that is, propane) limits the diffusion of the gas mixture through the capillaries. [g] The fugacity of the gas mixture is estimated through Lewis and Randall rule (similar to Dalton's law, but for the fugacity), $f = 0.92 f_{CH4} + 0.08 f_{C3H8}$, in molar basis. [h] The equilibrium pressure related to the system temperature is estimated through CSMGem[65–68], which gives values of $P_{eq,\mathrm{CH4}} = 31.7\times10^5$ Pa at 2°C, $P_{eq,\mathrm{mixture}} = 6.8\times10^5$ Pa at 2°C, and $P_{eq,\mathrm{mixture}} = 24.3\times10^5$ Pa at 12.5°C. The fugacity is then evaluated through RefProp[58]. [i] For the cases without additive, the oil-water interfacial tension is estimated through Antonoff rule[69], $\sigma_{w/o} = |\sigma_w - \sigma_o|$. No characterization of interfacial properties is available with the presence of additives, but it is considered that the additive cause the oil-water interfacial tension to decrease by ~ 25%, whereas the wetted angle is kept constant.

Table 2. Characteristics of rock-flow cell apparatus of Kakitani et al.[46,47] and input values that are kept constant in all experimental cases.

| | |
|---|---|
| Rock-flow cell inner diameter | 50.8 mm (2 in) |
| Rock-flow cell length | 0.5 m |
| Maximum inclination angle of rock-flow cell | 20° |
| Pressure | 70 bar |
| Volume of rock-flow cell | 1 L |
| Liquid loading | 50% (0.5 L of liquid) |
| Water cut | 10% (50 mL of water) |
| Initial particle radius[a] | ~ 1 mm |
| Liquids | Deionized water, mineral oil |
| Gas | Methane |
| | Gas mixture composed of 92% of methane and 8% of propane (molar basis) |
| Additive[b] | None // 1% mass |

[a] Approximate initial particle size-scale from experiments. Some experiments present stratification and/or formation during shut-in (stratified, static system), which evolve to particle radius in the mm-scale after few minutes. [b] Arquad® 2HT-75 from Sigma-Aldrich[70].

Table 3. Experimental tests of Kakitani et al.[46,47]

| Case[a] | #1 | #2 | #3 | #4 | #5 | #6 | #7 |
|---|---|---|---|---|---|---|---|
| Gas[b] | $CH_4$ | Mix | Mix | Mix | Mix | Mix | Mix |
| Temperature [$^oC$] | 2 | 12.5 | 2 | 2 | 2 | 12.5 | 2 |
| Subcooling [$^oC$] | 7.5 | 7.5 | 18 | 18 | 18 | 7.5 | 18 |
| Rotation of rock-flow cell [rpm] | 16 | 16 | 6 | 11.25 | 16 | 16 | 16 |
| Estimated shear rate[c] [$s^{-1}$] | 7 | 7 | 3.4 | 5.8 | 7 | 7 | 7 |
| Additive [% mass] | 0 | 0 | 0 | 0 | 0 | 1 | 1 |
| Agglomeration trend[d] | 1 | 1 | 3 | 3 | 3 | 2 | 3 |

[a] In the PhD of Kakitani[47], the numeration of the experimental cases is different, having the following correspondence: #1 = 4, #2 = 7, #3 = 8, #4 = 9, #5 = 10, #6 = 13, #7 = 16. [b] 'Mix' stands for the gas mixture of 92% of methane and 8% of propane (in mol). [c] The shear rate is approximated by turbulent velocity profiles of single-phase, steady-state, developed flow in smooth pipes (see demonstration #5 of the Supporting Information). [d] See section 4. Trend 1: stable agglomerate size of ~12 mm after ~1 h. Trend 2: stable agglomerate size of ~6 mm after ~40 min. Trend 3: no agglomeration, particles remain the ~1 mm scale.

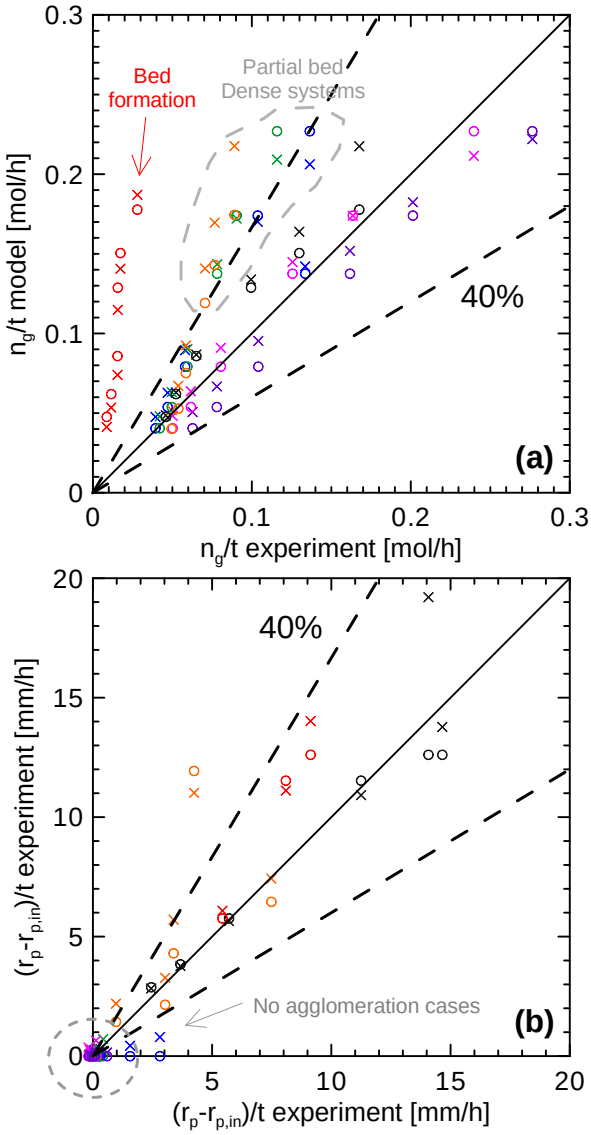


Figure 5. Comparison of the model with experimental data for (a) the average gas consumption rate $(n_g/t)$ and (b) the average rate of particle radius increase $[(r_p - r_{p,in})/t]$, evaluated at time instants 20 min, 40 min, 1 h, 2 h, 3 h, and 4 h after hydrates onset. Cross = complete model, circle = simplified model, black = case #1, green = #2, orange = #3, magenta = #4, red = #5, blue = #6, purple = #7.

## 4. Agglomeration Trends Captured by the Model

In this section, the trends captured by the model are discussed and compared to visualization of the rock-flow cell experiment. Figure 6 shows schematics of the behavior of gas consumption and

particle/agglomerate radius evolution in time for the experimental dataset tested, compared to photos of the rock-flow cell experiment. Figure 7 presents the comparison of experiment, complete model, and simplified model (to be introduced in section 5; for instance, neglect the dashed lines) for three selected cases.

Gas consumption behaves approximately in the same way for all experiments, reaching an asymptote of ~ 0.15-0.25 mol after 4 h. It is important here to emphasize that, if the experiment is maintained for a time scale of one order of magnitude higher (e.g., 1 day), then a new asymptote is reached; and if the time scale is again increased in one order of magnitude (e.g., 1 week; see experiments of Turner et al.[71] in this time-scale), then a new asymptote is reached again. However, the exponential mathematic function to model the porosity evolution reaches, at some point, an asymptote, and the value of the asymptote reached depends on the experimental dataset used to regress $\alpha_p, \lambda$. Here, the time-scale of 4 h was used, which implies that, if ever the gas consumption model is used to predict times-scales larger than that, then the model will erroneously predict an asymptote after 4 h. The time-scale chosen is representative of the flow inside pipelines (e.g., a 15 km pipeline at a mixture velocity of 1 m/s). Another important fact is that the model overpredicts gas consumption when bed formation occurs, noticeable for case #2 (marked in red in Figure 5, and pointed out in Figure 6). Bedding incurs in a decrease of the particle-bulk interfacial surface and in variation on the particle deformation / water squeezing / cracking of new capillaries coupled phenomena. Other cases (namely #1,3,4,6) present minor deviations from the exponential gas consumption predicted by the model, those related to partial bed formation or to dense systems / larger agglomerates in systems where agglomeration is more pronounced (low subcooling) and when shear rate is smaller. The gas consumption model behaves better for the dispersed systems (no agglomeration, that is, high subcooling, and when shear rate is high), namely cases #5 and #7. As a main conclusion, the growth kinetic model hypothesis of homogeneously dispersed system causes a higher particle-bulk interfacial surface (a larger number of smaller particles), thus overpredicting the gas consumption for scenarios of non-dispersed flow, and therefore the gas consumption model can be said *conservative*. As well, *discontinuities in gas consumption can be used to experimentally determine the existence of bed formation and/or heterogeneous/dense dispersions*.

The agglomeration model, by its turn, presents mainly three trends for the experimental dataset considered:

- Trend 1: stable agglomerate radius of ~12 mm, reached after ~1 h, related to low subcooling cases without additive.
- Trend 2: stable agglomerate radius of ~6 mm, reached after ~40 min, related to low subcooling cases with additive, showing the effect of lower interfacial properties into decreasing agglomeration.
- Trend 3: no agglomeration, particles remain in the same order of magnitude of ~1 mm for the entire experiment, related to high subcooling cases, showing its effect into drying out the particles.

Two observed phenomena are not captured by the agglomeration model. The first is the fact that some larger, unstable structures may appear in the first minutes after the onset of formation, as pointed out in Figure 6. This causes an initial peak in the particle radius curve (see schematics in Figure 6 and experimental data in Figure 7b). These structures are associated: (i) to the transient evolution of the flow pattern, especially due to the restart process of Kakitani et al.[46,47] experimental procedure (notice that they were interested on formation during shut-in/restart processes, and when it occurs in the restart, then the system takes a few minutes to reach a steady flow pattern, during which this anomalous large structures were observed), or (ii) to a free water phase that, during few minutes, is still not entrapped by the porous particles (that is, there is not yet sufficient porous media to trap all the water), causing particles to be wet due to the existence of a free water phase. Both (i) and (ii) are not considered in the model.

The second phenomena not captured (and not considered) by the agglomeration model is the breakage of the large agglomerates into fine particles at the end of the experiment (usually observed after 2 h), called *attrition*. These fine particles will not jam and not lead to a quick plugging of the flow line, and represent the ideal slurry flow sought for hydrate management. The slurry flow is however related to increase in the mixture apparent viscosity, an aspect widely treated in literature[15,17,29,72–75] and that is not the focus in this article.

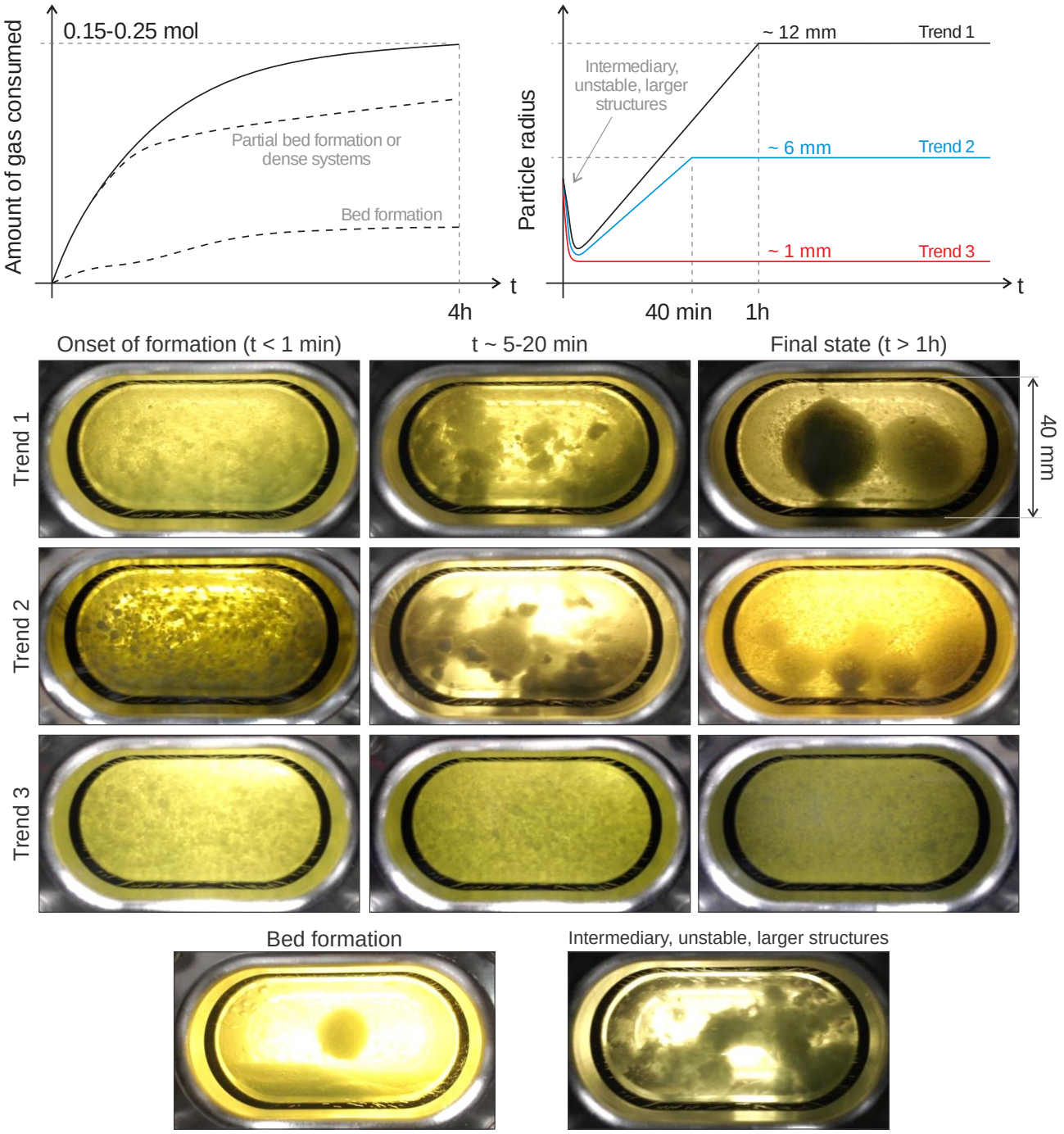


Figure 6. Schematics of the model behavior for the amount gas consumed and particle/agglomerate radius evolution in time, compared to photos of the system morphology.

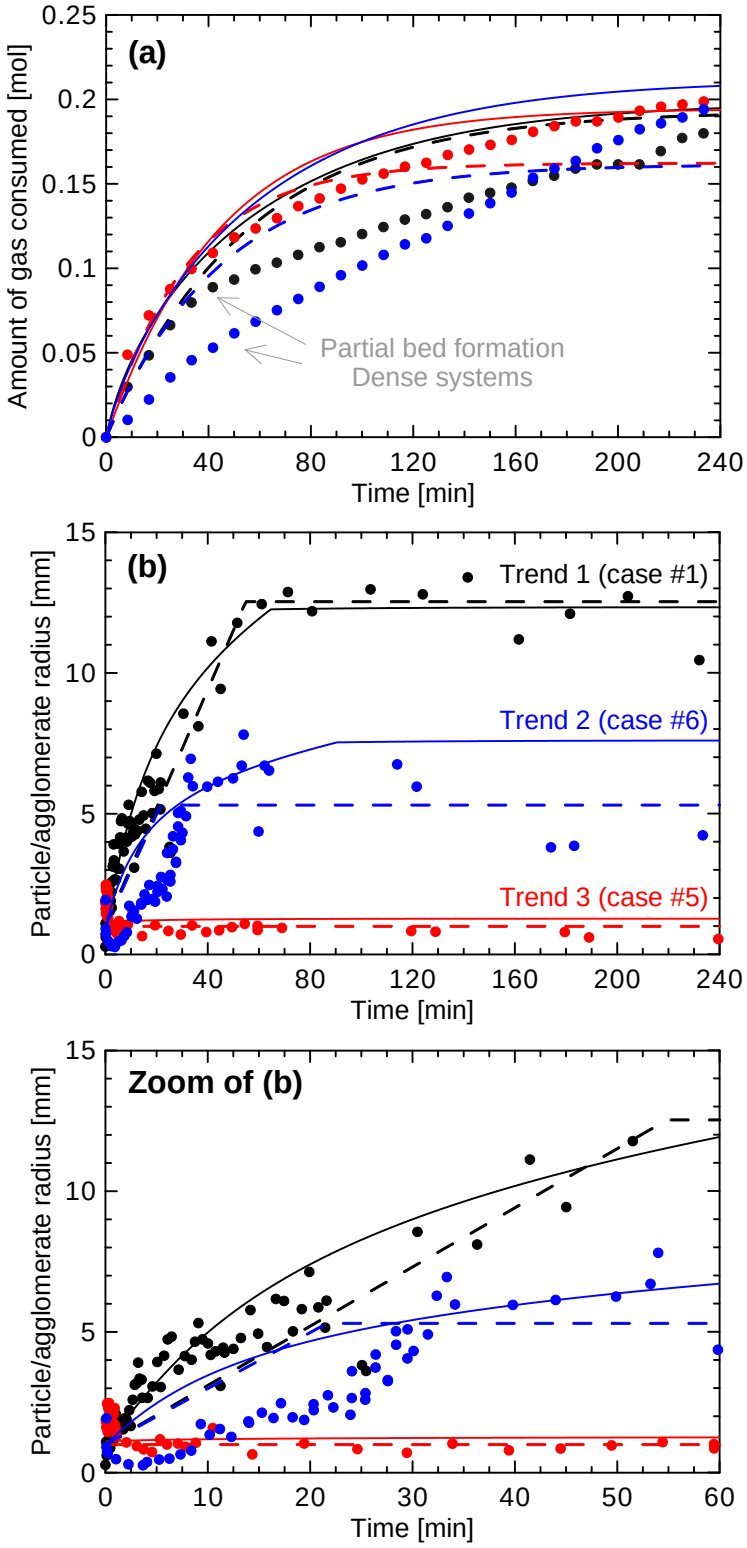


Figure 7. Comparison between experiments (circle), complete model (continuous line) and simplified model (dashed line). (a) Amount of gas consumed in time, where the model overpredicts when bed forms and/or when the system is dense (mostly for low subcooling and low shear rate).

(b) Particle/agglomerate radius evolution in time, showing the three discussed trends. Selected cases: #1 (black), #5 (red) and #6 (blue).

***Influence of Driving Force (Subcooling)***

The values of $\alpha_p, \lambda$ were experimentally regressed for case #1, whereas all other closure parameters were equal to the values of part II[2], besides the initial porosity, considered to be $\varepsilon_{in} = 90\%$. The same closure of case #1 (methane hydrate, structure I) was extrapolated to case #2 for the gas mixture hydrate (structure II), showing good results. When extrapolating the same closure to case #5 (gas mixture, equal to case #2, but for higher subcooling), the model predicts a smaller stable agglomerate of ~11 mm, which is far larger than the experimental data (stable agglomerate size of ~1 mm, that is, system does not agglomerate, red line of Figure 7b). Therefore, there is a secondary mechanism of the influence of the subcooling in agglomeration that needs to be considered, as discussed next.

Figure 8a shows a theoretical plot of the kernel of agglomeration against the subcooling. It is observed higher driving forces actually enhances agglomeration because of faster consolidation. However, from experimental observation, the stable agglomerate size decrease, which let us conclude that the predominant mechanism is that higher driving forces cause particles to dry out faster, thus reducing the time window where agglomeration happens (an expression for the time the particle takes to dry out is developed in section 5). The wet vs dry criterion, eq (27), is very sensitive on the porous medium parameters, and *it is known that the porous medium morphology can drastically change depending on the subcooling*.

Higher subcooling promotes higher initial porosity, smaller capillary radius, higher tortuosity, and smaller interconnectivity. These porous media / driving force interactions occur in size- and time-scales much smaller than the ones considered in the model, and therefore are not captured by it. Since tortuosity shall not vary too much (see discussion in Dullien[61], which states that abnormally large tortuosity fitted from experiments are most probably due to the non-consideration of interconnectivity of the capillary bundle), and that the model is sensitive to both the initial porosity and capillary radius (see Figure 12c-d of part II[2]), then we considered only variations on the porous medium interconnectivity.

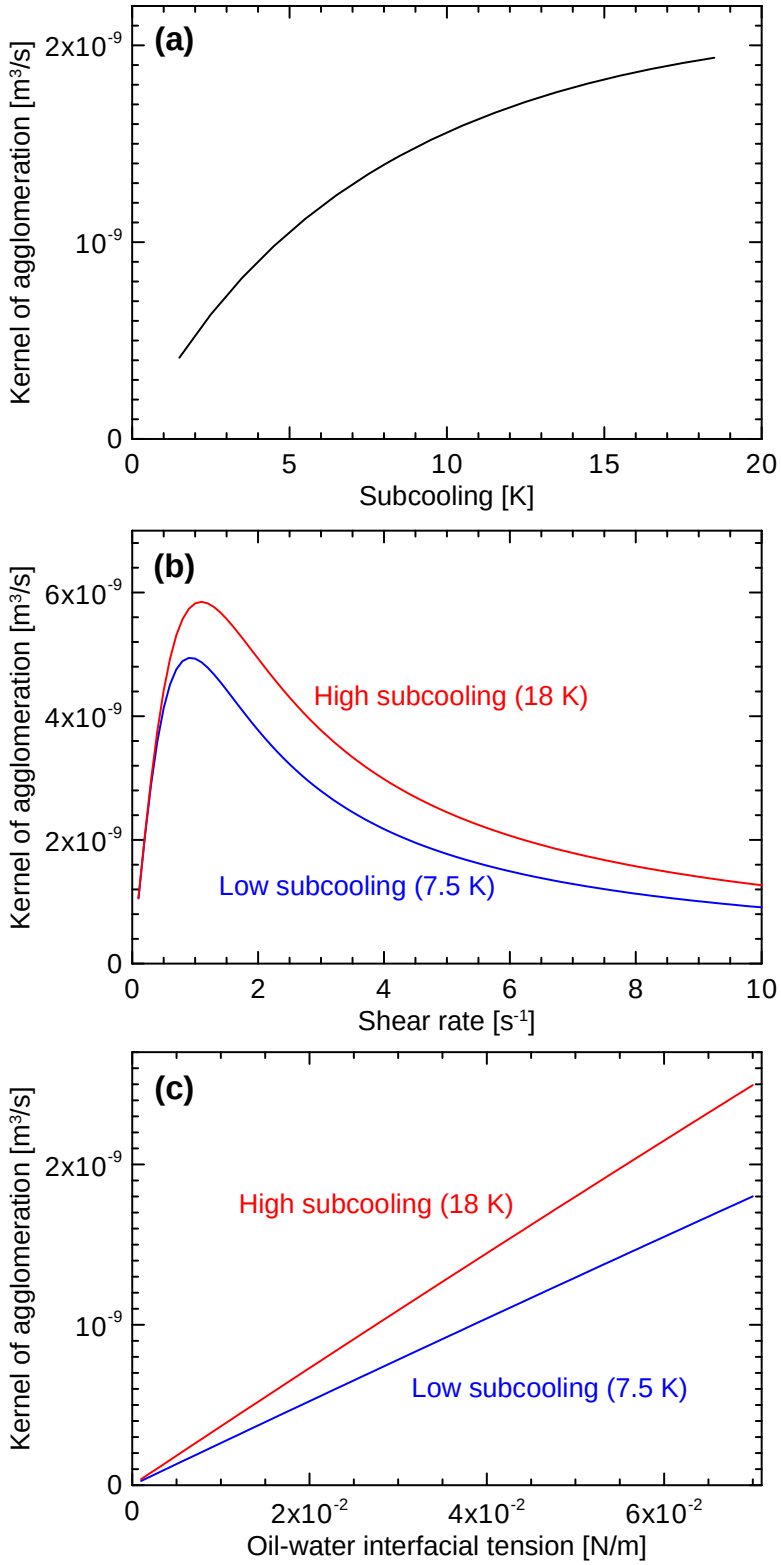


Figure 8. Theoretical curve of the kernel of agglomeration dependence on: (a) subcooling, (b) shear rate, and (c) oil-water interfacial tension. Evaluated from eq (26) considering the gas mixture; the moments of particle size distribution are evaluate at the initial condition, $t = 0$, from eq (9), and

considering the initial particle size of 1 mm; the linear growth rate comes from eq (7), evaluated at $t = 0$, where $\varepsilon = \varepsilon_{in} = 90\%$, with $G \approx 1.7 \times 10^{-7}$ m/s for the 7.5 K subcooling case, and $G \approx 2.4 \times 10^{-7}$ m/s for the 18 K subcooling case; gas fugacity comes from RefProp[58] evaluated at $(P,T)$ for the free gaseous phase and at $(P_{eq},T)$ for the equilibrium gas-water-hydrates; equilibrium pressure comes from CSMGem[65–68]; mixture fugacity evaluated using Lewis-Randal rule; interfacial properties evaluated without additive.

The porous medium interconnectivity is related to a certain number of capillaries having partial or complete restrictions, or to the fact that the capillary bundle has non-uniformities (different capillary radii) connected in series or in parallel. Both incur in variations of the permeability of the porous particle, that is, both are able to change the time taken for the particle to dry out. In part II[2], we proposed a range of interconnectivity varying in between $0.001 \le \zeta \le 0.02$. The highest value of interconnectivity is therefore adopted for the case of low subcooling (7.5 K), and the smaller value for the case of high subcooling (18 K). From Figure 7b, it is observed that, by using a smaller interconnectivity, the particles are dry from the onset of their formation, thus avoiding agglomeration. Therefore, the particle remains in the ~1 mm-scale over the entire simulation. As a conclusion, *the subcooling itself does not drastically changes the wet vs dry criterion or the kernel of agglomeration, but its effect on the porous medium parameters cause the time the particle takes to dry out to drastically decrease* (more is discussed in section 5).

From the experimental observation that higher subcooling cause better dispersed systems, it is fair to discuss the following *design paradox*. Heavy pipeline insulations are often adopted, among other objectives, to delay the onset of hydrate formation by maintaining high temperatures, which can incur in hydrate avoidance if the line is not so long, or if the temperature at the pipe entrance is high, or if the system pressure is not so high. But, *if ever hydrates form during production and a hydrate management strategy is sought, then the heat release due to hydrate formation is not transferred through the wall because of the heavy insulation, causing the mixture to reheat towards the equilibrium temperature. That is, heavy insulations cause low subcooling, thus the porous particles take much longer time to be sealed, and the particles remain wet for longer time, causing larger agglomerates. In other words, the use of heavy pipeline insulation, at least from our model*

*herein analyzed and concerned with hydrates only, will imply in the formation of large agglomerates that are most likely to plug the pipeline*.

It is yet important to comment about the behavior of the gas consumption model. It is experimentally observed that the increase in the subcooling cause no significant variation in the order of magnitude of gas consumption. The model however predicts higher gas consumption (see sensitivity analysis in Figure 12a of part II[2]), besides that, when the system remains dispersed, the particle-bulk interfacial surface is larger. Both cause predicted gas consumption to more than double for the cases of high subcooling compared to the cases of low subcooling. Since this is not experimentally observed, then it points out to an influence of the subcooling in the efficiency of the particles interacting with the bulk $\alpha_p$. In order to fit the experimental data, $\alpha_p = 0.06$ was regressed for the high subcooling cases. This smaller value is explained by a higher competition between the particles when the system is more dispersed (higher number of particles) and when the subcooling is higher.

***Influence of Shear Rate (Agitation)***

The closure of case #5 is used to simulate cases #3-4 for lower shear rates at high subcooling. Since the subcooling is kept high in cases #3-5, they do not present important agglomeration. As well, from the method used to capture the particle size (manual treatment of photos, that is, small statistic sample, and by using camera lenses that do not allow good observation of structures smaller than 1 mm), conclusions on the stable agglomerate size for shear rate variations cannot be retrieved.

Notice that all the cases of lower shear rates at low subcooling of Kakitani et al.[46,47] database incur in bed formation, thus are not herein tested since they are out of the range of applicability of the model. Therefore, *shear rate (agitation) is considered to be important into determining bedding when agglomeration is important (that is, low subcooling systems)*. Notice that shear rate also does not affect directly the gas consumption, since it affects the gas-bulk absorption resistance and the particle-bulk mass transfer resistance only, and both are negligible phenomena when considering hydrocarbon gases in oil-continuous flow, since these gases are much more soluble in oil than in water (see section 4.3 of part II[2]). Shear rate can however affect indirectly the gas consumption, since lower shear rates cause bed formation, thus decreasing gas consumption (as already discussed,

by a decrease in the particle-bulk interfacial surface, and/or by affecting water squeezing from the porous particle and micro-cracking of new capillaries).

Notice that the dataset used has a small variation in the agitation (shear rate) of the system. For larger variations, it is expected that the efficiency of particles interacting with the bulk ($\alpha_p$) increase with system agitation, increasing the gas consumption. For the agglomeration process, a theoretical curve of the kernel agglomeration vs shear rate is plotted in Figure 8b. It can be observed that two competitive phenomena occur: (i) up to ~ 1 $s^{-1}$, the kernel of agglomeration increase with shear rate due to an increase in the collision rate, and (ii) for > 1 $s^{-1}$, the kernel of agglomeration decrease with the shear rate due to an increase of the disruption rate. From this theoretical analysis, the experimental dataset is inside the range controlled by the disruption rate. Although the analysis show a decrease of the kernel of agglomeration by a factor of approximately ½ when going from a shear rate of 3.4 to 7 $s^{-1}$ (6 to 16 rpm in the oscillation rate of the rock-flow cell), the experimental results show insensitive to this variation, since the particles are dry from the onset (notice that the kernel of agglomeration plotted in Figure 8 is for considering a wet particle, since $K_{agg} \approx 0$ for a dry particle, that is, no liquid bridge holding the aggregate together).

For the low subcooling case, shear rate is therefore expected to influence agglomeration, but the large agglomerates will quickly tend to settle down, forming a bed. As a conclusion, *the shear rate (system agitation) is secondary on predicting agglomeration (subcooling is more important), having no influence when particles dry out fast (high subcooling); and being mostly important on determining bed formation and not agglomeration when particles take longer time to dry out (low subcooling).*

***Influence of Surfactant Additives (Interfacial Properties)***

The closure of case #2 is used to simulate case #6 (7.5 K subcooling, but with 1% mass of additive), and of case #5 to simulate case #7 (18 K subcooling, but with 1% mass of additive). Figure 7b shows that the use of 1% mass of additive (blue line) caused the stable agglomerate size to decrease by half of its size (blue line, trend 2) comparing with the case without additive for the low subcooling case (black line, trend 1). For the case of high subcooling, the agglomeration is avoided the same way, thus no substantial variation was observed by the introduction of the additive (red line, trend 3).

Additives usually present surfactant properties, which incur: (i) in lower oil-water interfacial tensions; (ii) in higher oil-water-hydrate wetted angles (water side), 'flattening' the oil-water meniscus inside the capillaries of the porous structure ($\theta_{o/w/h} = 90^o$ is a completely flat interface) or even inverting the nature of gas hydrates from hydrophilic to oilphilic (for $\theta_{o/w/h} > 90^o$), see Figure 5 of part I[1]; and (iii) in variations of the equilibrium curves of gas hydrate formation, thus changing the driving force (subcooling). Interfacial and equilibrium properties were not measured for the system with the insertion of the additive. As a theoretical analysis of the model, the oil-water interfacial tension is considered to decrease by ~25% by the use of 1% of additive, whereas no influence on the wetted angle and on the equilibrium curves is considered. By this consideration, the model is able to capture trend 2 when additive is added at low subcooling (blue line of Figure 7b).

Figure 8c presents a theoretical plot of the kernel of agglomeration against the oil-water interfacial tension. Lower oil-water interfacial tensions cause lower kernel of agglomeration, explained by a weaker liquid bridge holding the aggregate together. For the 25% decrease in the oil-water interfacial tension considered, the kernel of agglomeration decreases by approximately 40%. A second mechanism on decreasing the stable agglomerate size consists on smaller water permeation rates due to lower interfacial tensions, thus making particles to dry out faster. This will be further discussed in the next section.

## 5. Simplified Agglomeration Model for Gas Hydrates in Oil Continuous Flow

The aim of this section is to propose a simplified, engineering-oriented model for the time the particles take to dry out, for the particle/agglomerate size evolution in time, and for the stable (maximum) agglomerate size. The main simplification is that all moments of the particle size distribution are approximated to a representative order of magnitude along the entire process of agglomeration (see proof of hypothesis in demonstration #6 of the Supporting Information). This is necessary to avoid the solution of the system of ODEs of the population balance, eqs (6). Eqs (6) are simplified to the moments of $0^{th}$ and $1^{st}$ order only, and for the agglomeration term only, recognized as being the main process of increasing the particle size in time. By recognizing that $r_p = \frac{M_1}{M_0}$, by deriving it in time, by substituting the expressions for $\frac{dM_0}{dt}, \frac{dM_1}{dt}$ coming from

simplified eqs (6), and by further integrating while recognizing that $a_1 K_{agg} \approx cte$, the particle/agglomerate radius evolves linearly in time as (see demonstration #7 of the Supporting Information)

$$r_p = r_{p,in} + a_1 K_{agg} t \tag{28}$$

where $a_1 = \left(\frac{1}{2} + K_1\right)\bar{M}_1$, and $\bar{M}_1$ is a representative order of magnitude of the moment of first order of the particle size distribution. The kernel of agglomeration, eq (26), is simplified to the variables of interest (subcooling, shear rate, interfacial properties, oil properties, gas component properties) as

$$K_{agg} \approx a_2 \dot{\gamma} \left[ 1 + \frac{a_3}{k_{fT} \Delta T} \frac{\mu_o \dot{\gamma}^2}{\sigma_{o/w}} \right]^{-1} \tag{29}$$

where $a_2 = \frac{32}{3}\left(\frac{\bar{M}_1}{\bar{M}_0}\right)^3$ and $a_3 = (1-\varepsilon)\frac{g_4}{a_4}\frac{\bar{M}_3}{\bar{M}_2^2}$. Notice that the linear growth rate $G$, eq (7), is simplified by considering: (i) that when particles are agglomerating, they are wet, therefore the crystal integration (second term of the minimum function) is the limiting step for outer growth, and (ii) that when considering a gas much more soluble in oil than in water, and that oil is the continuous phase, then the particle-bulk mass transfer resistance is negligible $(h_{m,p/b} \to \infty)$, as well as the gas-bulk absorption resistance $(C_b \approx H_o f_g)$, as concluded from part II[2]. Therefore, the linear growth rate becomes $G \approx a_4 \Delta f$, where $a_4 = \frac{(\eta+1)}{(1-\varepsilon)}\frac{M_h}{\rho_h} k_i$. For further simplification, the driving force in fugacity is related linearly to the subcooling as $\Delta f \approx k_{fT} \Delta T$, where index '*fT*' stands for the transformation of fugacity driving force into subcooling. Table 4 presents the adopted values of $k_{fT}$.

Since the shear rate $\dot{\gamma}$ is hard to evaluate, we stick to Kolmogorov's theory, which considers a proportionality of the shear rate to the energy dissipation rate $\varepsilon_t$, which by its turn depends on the average mixture velocity $U$ and on the pressure gradient $\frac{dP}{dz}$. By the use of a known friction factor $f$ (in the Fanning representation), the relationship depends only on the mixture velocity

$$\dot{\gamma} = \sqrt{\frac{\rho_o}{\mu_o}\varepsilon_t} = k_{Kolm}\sqrt{\frac{U}{\mu_o}\frac{dP}{dz}} = k_{Kolm}\sqrt{\frac{2\rho_o f U^3}{\mu_o D}} \tag{30}$$

where the order of magnitude of the friction factor is approximated to single-phase, steady-state, developed flow in smooth pipes (Blasius) as

$$f = 0.0791\,\mathrm{Re}^{-0.25} \text{ with } \mathrm{Re} = \frac{\rho_o U D}{\mu_o} \tag{31}$$

where $\mathrm{Re}$ is the Reynolds number. The factor of proportionality $k_{Kolm} \approx 1$ is valid for laminar flow, or turbulent flow in the Kolmogorov size-scale, or turbulent flow close to the wall. For turbulent flow far from the wall, $k_{Kolm} \approx -1.25\omega + 0.57$ is found by the evaluation of a turbulent velocity profile in the geometry of the rock-flow cell and for an oil of 10 cP (see demonstration #5 of the Supporting Information). The velocity for the rock-flow cell case is evaluated as $U = 2\omega L$, where $\omega$ is the oscillation rate of the rock-flow cell (in Hz) and $L$ is the rock-flow cell length. Notice that this expression of $k_{Kolm}$ is very specific for the rock-flow cell apparatus in the conditions tested, but will further get absorbed by the parameters that need regression once extension to other experimental databases is done.

The criterion to determine if a particle is wet or dry, eq (27), is used to estimate the time taken for a particle to become dry. This happens when eq (27) equals unity

$$a_5 \sigma_{o/w} \cos\theta_{o/w/h} \frac{\zeta_{(\Delta T)}}{k_{fT}\Delta T}\varepsilon = 1 \tag{32}$$

where $a_5 = \frac{1}{12}\frac{\rho_w}{\mu_w M_w}\frac{1}{\eta\tau^2 k_i}\frac{\bar{M}_0}{\bar{M}_1}$. In this derivation, the porous medium interconnectivity is considered to be inversely proportional to the driving force by a sigmoid function called generalized logistic function or Richard's curve

$$\zeta_{(\Delta T)} \approx \zeta_{\max} + \frac{\zeta_{\min} - \zeta_{\max}}{1 + \zeta_{\max}\exp\left[-a_6\left(\Delta T - \Delta T^*\right)\right]} \tag{33}$$

which captures two asymptotes, being $\zeta_{\min} = 0.001$ the minimum and $\zeta_{\max} = 0.02$ the maximum values of porous medium interconnectivity. Parameter $\Delta T^*$ is the subcooling at which the interconnectivity is supposed to reach values close to the magnitude of the minimum

interconnectivity, and $a_6$ is a shape parameter of the sigmoid curve that represents how fast is the transition from the upper value $\zeta_{\max}$ to the lower one $\zeta_{\min}$. Precise fitting of $a_6, \Delta T^*$ request a refined dataset including intermediary subcooling between 7.5 K and 18 K, but fair values from the data herein considered are $a_6 \approx 1\,\mathrm{K}^{-1}$ and $\Delta T^* \approx 15\,\mathrm{K}$ (see plots of eq (33) in demonstration #8 of the Supporting Information).

The time dependence of eq (32) comes from the particle surface porosity $\varepsilon$. As the porosity decreases with time due to the sealing of the capillaries, the particles dry out. Eq (32) of part II[2], evaluated at $t = t_{dry}$, is simplified to $\varepsilon = \varepsilon_{\text{in}} \exp\left[-a_7 k_{fT} \Delta T t_{dry}\right]$, where $a_7 = (1-\lambda)(\eta+1)\dfrac{M_h}{\rho_h}\dfrac{k_i}{r_c}$. This expression considers that the gas is saturated inside the water at the oil-water interface $C_{out,w} = C_{sat,w} = H_w f_g$, valid when gas-bulk absorption and particle-bulk mass transfer are negligible (for much higher gas solubility in oil than in water when oil is the continuous phase, concluded in part II[2]). Using $\varepsilon$ in eq (32) and solving for the time the particle takes to become dry

$$t_{dry} = \max\left\{0\ ;\ \frac{k_3}{k_{fT}\Delta T}\ln\left(k_4\sigma_{o/w}\cos\theta_{o/w/h}\frac{\zeta_{(\Delta T)}}{k_{fT}\Delta T}\right)\right\} \tag{34}$$

valid for $k_4\sigma_{o/w}\cos\theta_{o/w/h}\dfrac{\zeta_{(\Delta T)}}{k_{fT}\Delta T} > 1$, that is, when particles are wet at the onset of hydrate formation. Otherwise, the particle is dry from the onset and $t_{dry} = 0$, which is the reason why the maximum function was introduced. From eq (30) into (29), and then into (28)

$$r_p = r_{p,in} + \left\{k_5\sqrt{\frac{\rho_o f U^3}{\mu_o D}}\left[1+\frac{k_6}{k_{fT}\Delta T}\frac{\rho_o}{\sigma_{o/w}}\frac{fU^3}{D}\right]^{-1}\right\}t \tag{35}$$

for $t < t_{dry}$, which is an expression for the evolution of the particle/agglomerate radius in time. And finally from eq (34) in (35)

$$r_{p,\max} = r_{p,in} + \frac{k_7}{k_{fT}\Delta T}\sqrt{\frac{\rho_o f U^3}{\mu_o D}}\left[1+\frac{k_6}{k_{fT}\Delta T}\frac{\rho_o}{\sigma_{o/w}}\frac{fU^3}{D}\right]^{-1}\max\left\{0\ ;\ \ln\left[k_4\sigma_{o/w}\cos\theta_{o/w/h}\frac{\zeta_{(\Delta T)}}{k_{fT}\Delta T}\right]\right\} \tag{36}$$

for $t \geq t_{dry}$, which is an expression for the stable (maximum) agglomerate radius. The constants of proportionality were renamed from $k_3$ to $k_7$. By substituting the auxiliary variables $a_1$ to $a_7$ and $g_4$

$$k_3 = a_7^{-1} = \frac{1}{(1-\lambda)(\eta+1)} \frac{\rho_h}{M_h} \frac{r_c}{k_i} \tag{37}$$

$$k_4 = a_5 \varepsilon_{in} = \frac{1}{12} \frac{\rho_w}{\mu_w M_w} \frac{\varepsilon_{in}}{\eta \tau^2} \frac{r_c}{k_i} \frac{\bar{M}_0}{\bar{M}_1} \tag{38}$$

$$k_5 = \sqrt{2} k_{Kolm} a_1 a_2 = \frac{32\sqrt{2}}{3} k_{Kolm} \left( \frac{1}{2} + K_1 \right) \frac{\bar{M}_1^4}{\bar{M}_0^3} \tag{39}$$

$$k_6 = 2k_{Kolm}^2 a_3 = 2k_{Kolm}^2 \frac{(1-\varepsilon)^2}{k_i} \frac{\eta}{(\eta+1)^2} \frac{M_w}{M_h^2} \frac{\rho_h^2}{\rho_w} \left[ \frac{3(\sin\varphi_b)^2 - (2+\cos\varphi_b)(1-\cos\varphi_b)}{(1-\cos\varphi_b)(1-\sin\varphi_b)} \right] \frac{\bar{M}_3}{\bar{M}_2^2} \tag{40}$$

$$k_7 = k_3 k_5 = \frac{32\sqrt{2}}{3} k_{Kolm} \frac{\left(K_1 + 1/2\right)}{(1-\lambda)(\eta+1)} \frac{\rho_h}{M_h} \frac{r_c}{k_i} \frac{\bar{M}_1^4}{\bar{M}_0^3} \tag{41}$$

Notice that $k_1, k_2$ were used in eq (39) of part II[2] for the simplified growth kinetic model, repeated below by using the subcooling instead of driving force in means of fugacity, relation $\Delta f \approx k_{fT} \Delta T$, thus

$$-\left.\frac{dn_g}{dt}\right|_{hyd} = k_1 \mathrm{WC} \forall_L \sqrt{H_w D_w} \frac{k_{fT} \Delta T}{\bar{r}_p} \exp\left[ -k_2 (\eta+1) k_{fT} \Delta T \frac{M_h}{\rho_h} t \right] \tag{42}$$

where $k_1 = 6\alpha_p \varepsilon_{in} \sqrt{\frac{k_i}{2r_c}}$, $k_2 = (1-\lambda)\frac{k_i}{r_c}$ and $\bar{r}_p = f_{agg} r_{p,in}$, $\bar{r}_p$ being a representative order of magnitude of the particle radius along the agglomeration process. Notice that the simple fact of using the instantaneous value of $r_{p(t)}$ significantly distances the curvature of eq (42) to the experimental data, since eq (42) comes from considering a constant particle radius associated to a constant number of particles, and the simple fact of changing the average particle radius does not capture both phenomena. We propose $\bar{r}_p \approx f_{agg} r_{p,in}$, where $f_{agg}$ is a regressed factor that captures

an averaged effect of both particle radius and variation of number of particles due to agglomeration. Table 4 presents the suggested values for evaluating the simplified model.

Table 4. Regressed parameters of the simplified model.

$$k_1 = 3.8\times10^{-2}\alpha_p\varepsilon_{in}\left[\frac{\text{mol}}{\text{m}^2\text{sPa}}\right]^{1/2} \text{ with}$$

$$\alpha_p\varepsilon_{in} \approx \begin{cases} 1.8\times10^{-2}, \text{ for flow loop of part II} \\ 13.5\times10^{-2}, \text{ for rock-flow cell of part III, 7.5 K subcooling} \\ 5.4\times10^{-2}, \text{ for rock-flow of part III, 18 K subcooling} \end{cases}$$

$$k_2 = 8.2\times10^{-5}(1-\lambda)\ \frac{\text{mol}}{\text{m}^2\text{sPa}} \text{ with } (1-\lambda) \approx \begin{cases} 1.9\times10^{-2}, \text{ for flow loop of part II} \\ 0.8\times10^{-2}, \text{ for rock-flow cell of part III} \end{cases}$$

$$k_3 = 1.1\times10^{10} \text{ Pa.s}$$

$$k_4 = 2\times10^{10} \text{ m}^{-1}$$

$$k_5 = 8.5\times10^{-5} \text{ m}$$

$$k_6 = 2\times10^{7} \text{ m.Pa.s}$$

$$k_7 = 9.6\times10^{5} \text{ m.Pa.s}$$

$$k_{fT} = \begin{cases} 4.6\times10^5 \text{ Pa/K, for } CH_4 \text{ at } \Delta T \approx 7.5 \text{ K} \\ 5.8\times10^5 \text{ Pa/K, for } 0.92CH_4 + 0.08C_3H_8 \text{ at } \Delta T \approx 7.5 \text{ K} \\ 3.4\times10^5 \text{ Pa/K, for } 0.92CH_4 + 0.08C_3H_8 \text{ at } \Delta T \approx 18 \text{ K} \end{cases}$$

$$\bar{r}_p \approx f_{agg} r_{p,in} \text{ with } f_{agg} = \begin{cases} 2.5, \text{ for } \Delta T \approx 7.5 \text{ K} \\ 1, \text{for } \Delta T \approx 18 \text{ K} \end{cases}$$

***Evaluation of the Simplified Agglomeration Model***

The evaluation of the simplified model is straightforward. With the knowledge of the mixture velocity $U$ (for the rock-flow cell, $U = 2\omega L$), the friction factor is evaluated from eq (31). The values of $k_1 - k_7$, $f_{agg}, k_{fT}$ come from Table 4. The porous medium interconnectivity is estimated by eq (33). The time the particle takes to dry out comes from eq (34), the evolution of particle/agglomerate radius from eq (35), and the stable (maximum) agglomerate radius from eq (36). The amount of gas consumed $n_g$ comes from a 1st order discretization, $n_{g(t+\Delta t)} = n_{g(t)} + \frac{dn_g}{dt}\Delta t$, where the instantaneous gas consumption rate $\frac{dn_g}{dt}$ is estimated from

eq (42). Figure 5 shows deviations plots of the average gas consumption rate and the average rate of particle increase, which stays very close to the complete model (that is, the simplifying hypothesis hold) and inside the ±40% deviation range. The behavior of the gas consumed and particle radius evolution in time, compared to the experimental data and to the complete model, is shown in Figure 7.

Figure 9 presents the simplified model sensitivity into determining the evolution of the particle/agglomeration radius. Case #2 is plotted in black as reference, using $k_{fT} = 5 \times 10^5$ Pa/K for any subcooling. Notice that *these plots show the stable agglomerate size (asymptote), the time for the particle to dry out (time where asymptote is reached), and the kernel of agglomeration (proportional to the inclination of the straight line)*. Figure 9a shows that higher subcooling cause higher kernel of agglomeration due to higher consolidations rates, but present smaller times for particle to dry out (due especially to the decrease of the porous medium interconnectivity), thus incurring in smaller stable agglomerates. Agglomeration is avoided for subcooling higher than 11 K for this case of study.

Figure 9b shows the sensitivity to percentage reductions in the oil-water interfacial tension by, e.g., the use of a surfactant additive. Smaller oil-water interfacial tension cause smaller kernel of agglomeration due to a reduction in the force sticking the agglomerate together (the liquid bridge), thus increasing the disruption rate. Smaller interfacial tensions also incur in smaller water permeation rates through the particle, thus the time for particle to dry out is reduced. For oil-water interfacial tensions of $\sigma_{o/w} \leq 2 \times 10^{-2}$ N/m (reductions of 60% or more), agglomeration is avoided in the case of study.

Figure 9c shows the sensitivity to the oil-water-hydrate wetted angle (water side). The wetted angle does not influence the kernel of agglomeration. The use of surfactant additives increases the wetted angle (tends to invert affinity of hydrates from hydrophilic to oilphilic). Higher wetted angle causes smaller water permeation rate through the porous particles, thus reducing the time for the particle to dry out, and the system reaches smaller stable agglomerate sizes. For wetted angles of $80^o$ or higher, agglomeration is avoided in the case of study.

Figure 9d shows the sensitivity to the mixture velocity for 7.5 K of subcooling. The rock-flow cell oscillation rate relative to each velocity of the rock-flow cell is shown in parenthesis, and some velocities are extrapolated to real production scenarios (in the order of magnitude of 1-3 m/s). It is important to notice that, as already discussed, when the system agglomerates (low subcooling) and

the velocity (or the shear rate) is small, then bed formation is most likely to occur, which is not captured by the model. Even if Figure 9d is theoretical, it highlights that, for higher velocities, the kernel of agglomeration is reduced because of an increase in the disruption rate. In turn, the time taken for the particle to dry out is not influenced by the flow velocity, because it is dependent on mass transfer and driving force, and because mass transfer particle-bulk and gas absorption are not limiting steps of the crystallization. For high velocities, however, the efficiency of particles interacting with the bulk $\alpha_p$ is expected to increase and to affect the crystallization, thus affecting the time for the particle to dry out. This is however not captured by the model. Furthermore, at high velocities (high shear rate), breakage/attrition may be important, but those are also not considered in the model.

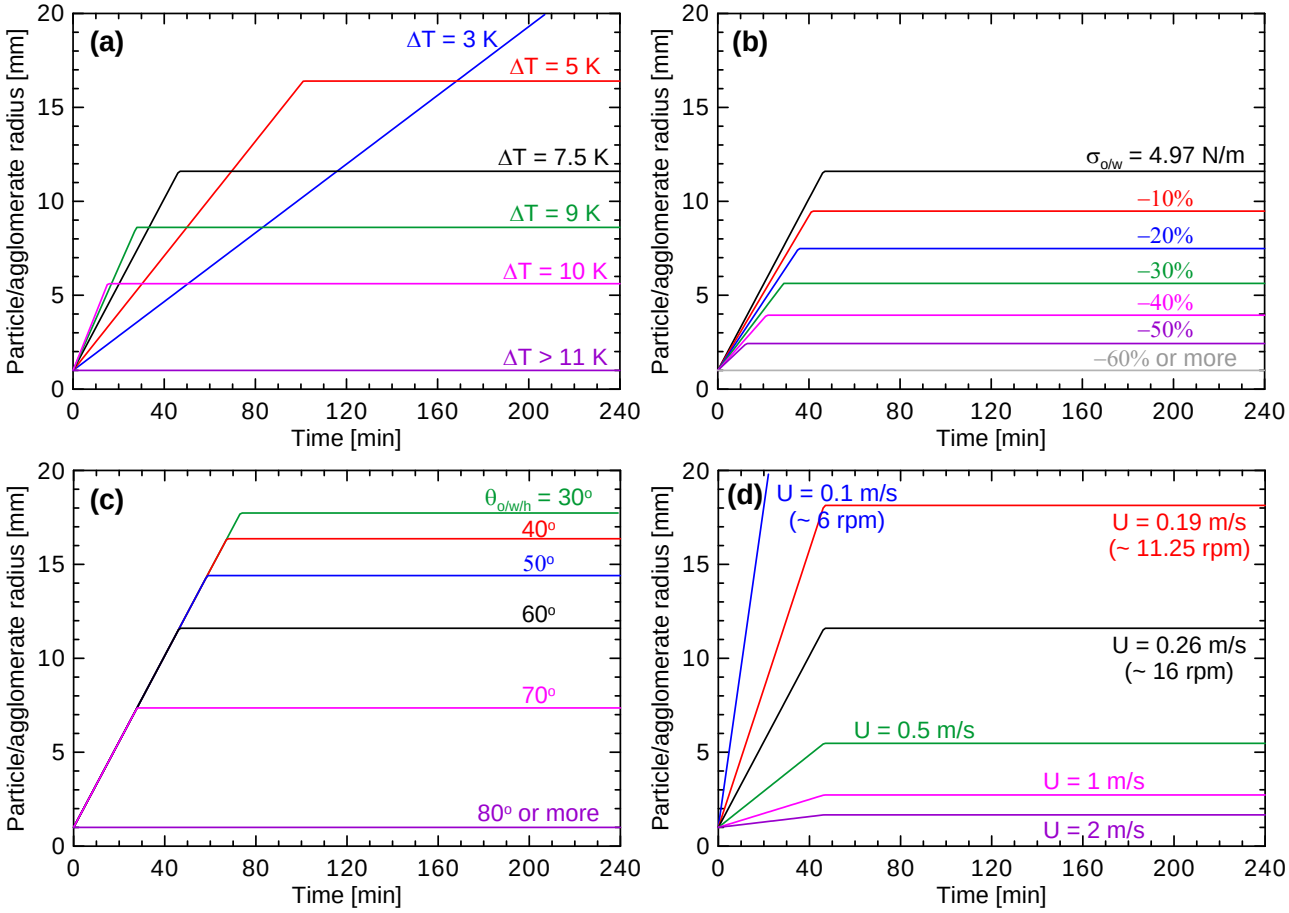


Figure 9. Particle/agglomerate radius evolution in time, estimated from the simplified agglomeration model. Sensitivity to: (a) subcooling, (b) oil-water interfacial tension, (c) oil-water-hydrate wetted angle (water side), and (d) flow velocity. In black, case #2 for $k_{fT} = 5\times10^5$ Pa/K.

Finally, Figure 10 presents (a) the time for particle to dry out, eq (34), and (b) the increase in the particle/agglomerate size, $(r_{p,\max} - r_{p,in})$ from eq (36), against the subcooling. It is observed that both present the same trend, a steep decrease with subcooling related to the decrease in the interconnectivity of the porous medium. Several lines are plotted for different oil-water interfacial tension and oil-water-hydrate wetted angle (water side). *Higher subcooling show to be the more important factor to avoid agglomeration, whereas lower interfacial properties are secondary*, which is in agreement with the experimental observations of the dataset of Kakitani et al.[46,47]

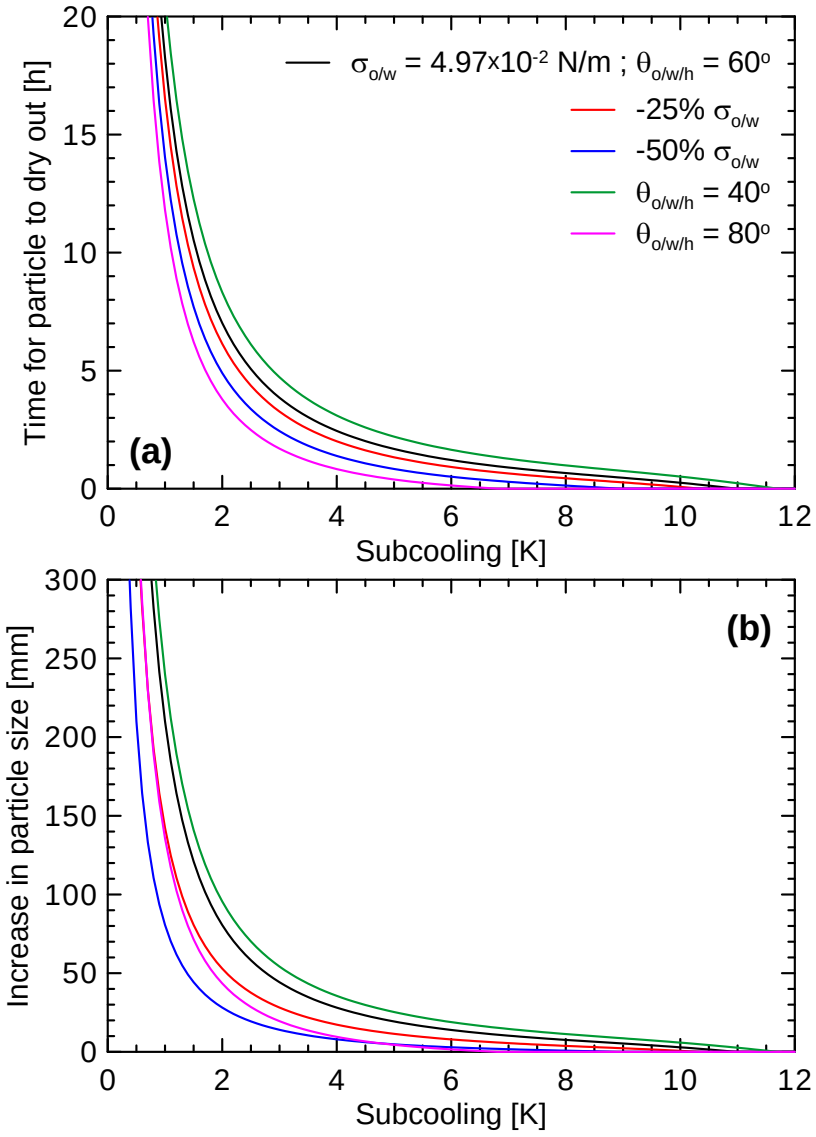

Figure 10. (a) Time for particle to dry out, eq (34), and (b) increase in particle/agglomerate size $(r_{p,\max} - r_{p,in})$, eq (36), against subcooling and for different oil-water interfacial tension and oil-water-hydrate wetted angle (water side).

***Development of a Criterion for Hydrate Dispersed Systems***

The problem is simplified one step further by the fact that, for hydrate management purposes, agglomeration shall be avoided at the maximum and, therefore, prediction of the agglomerate size itself is not necessary. What is necessary, instead, is a *criterion to understand if the system will be dispersed or not after the onset of hydrate formation*. And this is fairly simple given the herein developed model: *the system will not agglomerate when the time for particles to dry out is zero*, $t_{dry} = 0$, *that is, when particles are dry from the onset of their formation*. By making eq (34) equal to zero and by recognizing that $\ln(1) = 0$, the transition from a system that agglomerates to a system that remains dispersed when hydrates form is given by

$$\frac{\Delta T}{\zeta_{(\Delta T)}} = \frac{k_4}{k_{fT}} \sigma_{o/w} \cos\theta_{o/w/h} \tag{43}$$

where $\Delta T$ is the subcooling of the system, $\sigma_{o/w}$ is the oil-water interfacial tension, $\theta_{o/w/h}$ is the oil-water-hydrate wetted angle (water side), $\zeta_{(\Delta T)}$ is the interconnectivity of the porous medium (evaluated through eq (33), where $\zeta_{\min} = 0.001$, $\zeta_{\max} = 0.02$, $a_6 = 1$ and $\Delta T^* = 15\,\mathrm{K}$ is adopted in this study), $k_{fT}$ is the proportionality factor that transforms fugacity driving force into subcooling, and $k_4$ comes from eq (38), and its suggested value for the database tested comes is shown in Table 4.

Figure 11 present a plot of the subcooling $(\Delta T)$ against the product of the interfacial tension and wetted angle $(\sigma_{o/w} \cos\theta_{o/w/h})$, which depends on the oil composition, the water salinity, the system pressure and temperature, and especially on the use of additives. The continuous line represents eq (43), and separates the dispersed systems (dry particles) to the systems that agglomerate (wet particles) after the onset of hydrate formation. The dataset of Kakitani et al.[46,47] is represented by the crosses. This plot can be used in two distinct ways:

1. If the interfacial properties are known in the presence/absence of additive, then the subcooling needs to be designed in order to assure a dispersed system. The subcooling, in

turn, comes from the competition of heat release because of hydrate formation (from growth kinetics) and the heat transfer with the external medium (which depends on the pipeline insulation).

2. If the subcooling is known, then an additive that assures the correct interfacial properties need to be chosen.

We suggest further testing of criterion proposed in eq (43) prior to industrial application, especially in order to regress the necessary parameters $(k_4, \zeta_{\min}, \zeta_{\max}, a_6, k_{fT})$ for systems using crude oils, natural gases, brine, and additives. Furthermore, even if the system presents dry particles, those particles can still settle down promoting a moving or stationary bed depending on the flow shear (mixture velocity), although it is most likely that those particles will not stick to the wall since they are dry. Coupling with multiphase flow is necessary to predict if the slurry is transported suspended or settles down. This is the topic of the next parts of this series of papers.

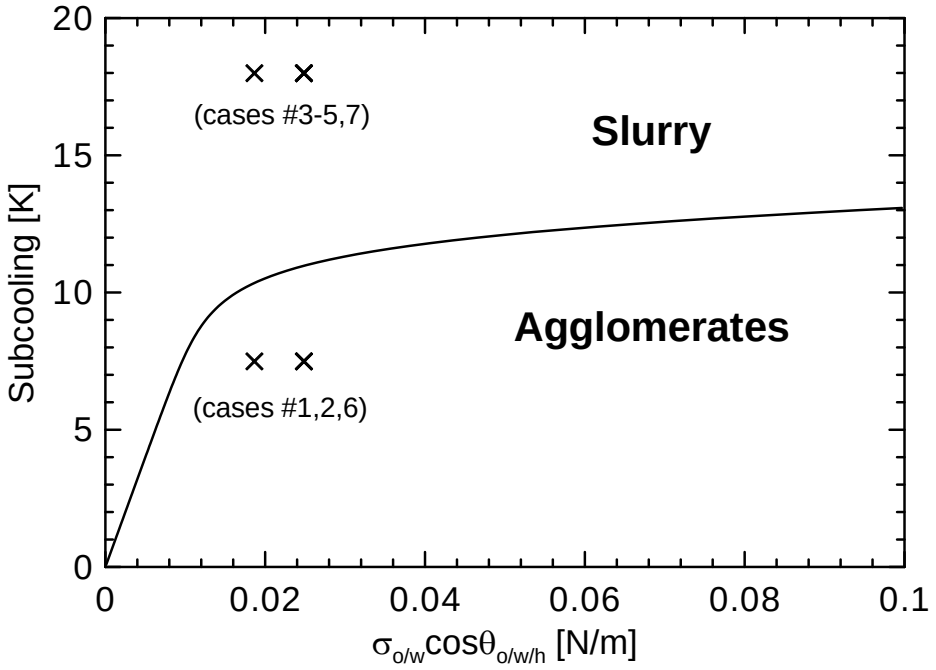


Figure 11. Criterion to predict if the system remains dispersed or if it agglomerates after the onset of hydrate formation. The line is the locus of $t_{dry} = 0$ for eq (43), that is, condition when particles are dry from the onset of hydrate formation.

## 6. Conclusions

This article is part III in the series for hydrate formation, agglomeration, and transportability in multiphase flow and it gives the mathematical description of the agglomeration process of hydrate particles in oil continuous flow in order to predict the evolution of the average agglomerate size in time. The model considers instantaneous nucleation, growth and agglomeration inside the population balance, solved by the Method of Moments, where the agglomeration depends on the collision, consolidation and disruption rate of particles. The disruption rate is modeled from the formation of a liquid bridge that holds the aggregate together. This, in turn, depends on the particle being wet or dry, which comes from the competition between water permeation through the porous hydrate particle and crystal integration in its outer surface. The model was compared to experiments and shows deviations in the ±40% range. The model was further simplified for gases with much higher solubility in oil than in water (hydrocarbon gases) in oil-continuous flow, giving rise to simple expressions for the time the particle takes to dry out, the evolution of the particle size, and the stable agglomerate size, and that give similar results when compared to the complete model. A simple criterion to classify if the system remains dispersed (slurry) or agglomerates is proposed. The following conclusions are gained from the model:

- Higher subcooling promotes faster sealing of the particles and relates to lower porous medium interconnectivity, which together cause the systems to behave more dispersed. This points out to a reevaluation of the use of heavy pipeline insulation when hydrate management strategy for slurry flow is sought.
- The use of surfactant additives causes lower oil-water interfacial tension and higher oil-water-hydrate wetted angle (water side), which both contribute to decrease the water permeation through the particle, leading to smaller time for the particle to dry out and, consequently, smaller stable agglomerates.
- The gas consumption model behaves well for dispersed, non-agglomerating systems. For denser systems, especially when bed formation occurs, the model overpredicts gas consumption. Discontinuities of the experimental gas consumption curve can point out the existence of bed formation and dense particulate flow.

The agglomeration model presented, including the simplified model and the developed criterion for dispersed systems, is one of the connecting pieces of our multiscale in multiphase flow approach. The next part in this series will describe the mathematics of the multiphase flow,

focusing in the prediction of pressure and temperature along the pipeline, which together give the subcooling for both the growth kinetics and agglomeration of gas hydrates.

## Supporting Information

The supporting information contains mathematical demonstrations of the model, notably demonstration of the population balance using the Method of Moments, and discussions on the hypothesis made, such as the use of the collision rate of Smoluchowski, the meaning and acceptable values for the agglomerate shape coefficients, the shear rate estimation from a turbulent velocity profile, and the validity of Kolmogorov relation for shear rate estimation in turbulent flow at the liquid bulk. This information is available free of charge via the Internet at http://pubs.acs.org/.

## Corresponding authors

*Amadeu K. Sum, asum@mines.edu
*Rigoberto E.M. Morales, rmorales@utfpr.edu.br
*Ana Cameirão, cameirao@emse.fr

## Acknowledgements

The research groups are part of the Joint International Research Program on Gas Hydrates and Multiphase Flow (JIRP). The authors acknowledge the financial support of Région AURA Auvergne Rhône-Alpes through the project COOPERA FluEnergy, the Institut Mines-Télécom, the Coordination for the Improvement of Higher Education Personnel - Brazil (CAPES) - Finance Code 001, and TE/CENPES/PETROBRAS (5850.0103370.17.9). CLB thanks Dr. Cesar Ofuchi for coding the image treatment software used to retrieve the agglomerate size evolution in time, Dr. Henrique Stel for the discussion on the shear rate estimation of the rock-flow cell, Eng. Fernando Fabiane for the information on the average flow shear rate retrieved from his CFD simulations of air-water flow in a rock-flow cell, and MSc. Fausto Arinos Barbuto for the discussion on the oil viscosity estimation for pressurized conditions.

**Nomenclature**

*Roman letters*

| | | |
|---|---|---|
| $A$ | Surface area | [$m^2$] |
| $a_1 - a_7$ | Auxiliary parameters of simplified model | |
| $A_{g/o}$ | Interfacial surface between gas and oil | [$m^2$] |
| $C_b$ | Gas concentration in the bulk | [$mol/m^3$] |
| $D$ | Pipeline/rock-flow cell inner diameter | [m] |
| $D_w, D_o$ | Gas diffusivity in water/oil | [$m^2/s$] |
| $f$ | Friction factor (Fanning) | [-] |
| $f(L,t)$ | Particle size distribution per unit volume | [$m^{-4}$] |
| $f_{agg}$ | Factor of the representative order of magnitude of particle radius relatively to initial particle radius due to agglomeration for the simplified model | [-] |
| $f_g$ | Gas fugacity in gaseous free phase evaluated at system pressure and temperature, $f_g(P,T)$ | [Pa] |
| $f_{eq}$ | Gas fugacity at gas-water-hydrate equilibrium, evaluated at system temperature and its related equilibrium pressure, $f_{eq}(P_{eq},T)$ | [Pa] |
| $g_1 - g_4$ | Geometric factors defined during modeling of the kernel of agglomeration | |
| $G$ | Linear outer growth rate of the particle, or particle growth velocity | [m/s] |
| $h_{m,p/b}$ | Mass transfer coefficient between particle and bulk | [m/s] |
| $H_w, H_o$ | Henry's constant of gas inside water/oil in the solubility form | [$mol/(m^3Pa)$] |
| $j$ | Order of the moment of particle size distribution | [-] |
| $k_1 - k_7$ | Parameters of simplified model | |
| $K_1, K_2$ | Agglomerate shape coefficients | [-] |
| $k_{abs}$ | Absorption coefficient of gas by the bulk | [m/s] |
| $K_{agg}$ | Kernel of agglomeration | [$m^3/s$] |
| $k_c$ | Consolidation rate | [$s^{-1}$] |
| $k_{col}$ | Collision rate | [$m^3/s$] |
| $k_d$ | Disruption rate | [$s^{-1}$] |
| $k_{fT}$ | Constant of proportionality between fugacity driving force and subcooling | [Pa/K] |
| $k_i$ | Constant of proportionality of crystal integration | [$mol/(m^2.s.Pa)$] |
| $k_{Kolm}$ | Constant of proportionality of Kolmogorov relation for shear rate | [-] |
| $L$ | Rock-flow cell length. Exception: represents the particle size scale when inside the particle size distribution $f(L,t)$ | [m] |
| $m$ | Mass | [kg] |
| $M$ | Molar mass | [kg/mol] |
| $M_j$ | Moment of $j^{th}$ order of the particle size distribution | [$m^{j-3}$] |

| | | |
|---|---|---|
| $\bar{M}_j$ | Representative value of the moment of j$^{th}$ order of the particle size distribution for the simplified model | [m$^{j-3}$] |
| $n_g$ | Molar amount of gas | [mol] |
| $n_p$ | Number of particles in the system | [-] |
| $n_{p,in}$ | Initial number of particles in the system | [-] |
| $-dn_g/dt\big\|_{hyd}$ | Total gas consumption rate due to hydrate formation (all particles) | [mol/s] |
| $-dn_{g,i}/dt\big\|_{hyd}$ | Gas consumption rate due to hydrate formation in one particle *i* | [mol/s] |
| $P$ | Pressure | [Pa] |
| Re | Reynolds number | [-] |
| Sc | Schmidt number | [-] |
| Sh | Sherwood number | [-] |
| $r_c$ | Capillary radius | [m] |
| $r_d$ | Droplet radius | [m] |
| $r_1, r_2$ | Radii of agglomerating particles | [m] |
| $r_p$ | Particle/agglomerate radius | [m] |
| $\bar{r}_p$ | Representative order of magnitude of particle radius for simplified model | [m] |
| $r_{p,in}$ | Initial particle radius | [m] |
| $r_{p,\max}$ | Stable (maximum) agglomerate radius | [m] |
| $t$ | Time | [s] |
| $T$ | Temperature | [K] |
| $t_c$ | Time-scale of consolidation | [s] |
| $t_{dry}$ | Time for particle to dry out | [s] |
| $\Delta t$ | Time step | [s] |
| $\Delta T$ | Subcooling | [K] |
| $\Delta T^*$ | Critical subcooling where the porous medium is considered to reach the minimum interconnectivity | [K] |
| $U$ | Velocity | [m/s] |
| $U_{p/b}$ | Relative velocity (slip velocity) between particle and bulk | [m/s] |
| $\forall$ | Volume | [m$^3$] |
| $\forall_L$ | Volume of liquid (oil + water) | [m$^3$] |
| WC | Water cut | [-] |

*Greek letters*

| | | |
|---|---|---|
| $\alpha_p$ | Efficiency of particles interacting with the bulk | [-] |
| $\dot{\gamma}$ | Shear rate | [s$^{-1}$] |
| $\varepsilon$ | Hydrate porosity (at outer surface of the particle) | [-] |
| $\varepsilon_{in}$ | Initial hydrate porosity (at outer surface of the particle) | [-] |
| $\varepsilon_t$ | Energy dissipation rate | [m$^2$/s$^3$] |

| | | |
|---|---|---|
| $\phi_1 - \phi_3$ | Geometric factors that relate average parameters of the particle to the moments | [-] |
| $\varphi_b$ | Polar angle wetted by the liquid bridge | [rad] |
| $\eta$ | Hydration number | [mols of $H_2O$ / mol of hyd] |
| $\eta_{agg}$ | Agglomeration efficiency | [-] |
| $\eta_{col}$ | Collision efficiency | [-] |
| $\lambda$ | Capillary birth-to-death ratio | [-] |
| $\mu$ | Dynamic viscosity | [Pa.s] |
| $\theta_{o/w/h}$ | Oil-water-hydrate wetted angle (water side), $\theta_{o/w/h} < 90^o$ (hydrophilic hydrates) | [rad] |
| $\rho$ | Density | [kg/m$^3$] |
| $\sigma_{o/w}$ | Oil-water interfacial tension | [N/m] |
| $\tau$ | Capillary tortuosity | [-] |
| $\omega$ | Oscillation rate of rock-flow cell | [rpm or Hz] |
| $\zeta$ | Interconnectivity of porous medium | [-] |
| $\zeta_{\min}, \zeta_{\max}$ | Minimum and maximum porous medium interconnectivity | [-] |

*Indexes*

| | |
|---|---|
| *abs* | Absorption |
| *agg* | Agglomeration |
| *b* | Bridge $(A_b, \forall_b, \varphi_b)$ or bulk $(C_b)$ |
| *c* | Capillary $(r_c)$ or consolidation $(k_c, t_c)$ |
| *col* | Collision |
| *d* | Droplet |
| *eq* | Three-phase gas-water-hydrate equilibrium |
| *g* | Guest of the gas hydrate, that is, gas (as a component, not as a phase) |
| *h* | Hydrate phase |
| *hyd* | Hydrate formation |
| *i* | Referent to one particle |
| *in* | Initial condition |
| *L* | Liquid (oil + water) |
| *o* | Oil |
| *out* | Outer surface of the particle |
| *p* | Hydrate particle |
| *sat* | Saturation |
| *w* | Water |

## References

(1) Bassani, C. L.; Melchuna, A. M.; Cameirão, A.; Herri, J.-M.; Morales, R. E. M.; Sum, A. K. A Multiscale Approach for Gas Hydrates Considering Structure, Agglomeration, and Transportability under Multiphase Flow Conditions: I. Phenomenological Model. *Ind. Eng. Chem. Res.* **2019**, *58* (31), 14446–14461. https://doi.org/10.1021/acs.iecr.9b01841.

(2) Bassani, C. L.; Sum, A. K.; Herri, J.-M.; Morales, R. E. M.; Cameirão, A. A Multiscale Approach for Gas Hydrates Considering Structure, Agglomeration, and Transportability under Multiphase Flow Conditions: II. Growth Kinetic Model. *Ind. Eng. Chem. Res.* **2020**, *59* (5), 2123–2144. https://doi.org/10.1021/acs.iecr.9b04245.
(3) Englezos, P.; Kalogerakis, N.; Dholabhai, P. D.; Bishnoi, P. R. R. Kinetics of Formation of Methane and Ethane Gas Hydrates. *Chem. Eng. Sci.* **1987**, *42* (11), 2647–2658. https://doi.org/10.1016/0009-2509(87)87015-X.
(4) Herri, J. M.; Pic, J. S.; Gruy, F.; Cournil, M. Methane Hydrate Crystallization Mechanism from In-Situ Particle Sizing. *AIChE J.* **1999**, *45* (3), 590–602. https://doi.org/10.1002/aic.690450316.
(5) Smoluchowski, M. v. Versuch Einer Mathematischen Theorie Der Koagulationskinetik Kolloider Lösungen. *Zeitschrift für Phys. Chemie* **1917**, *92* (1), 129–168. https://doi.org/10.1515/zpch-1918-9209.
(6) van de Ven, T. G. M.; Mason, S. G. The Microrheology of Colloidal Dispersions VII. Orthokinetic Doublet Formation of Spheres. *Colloid Polym. Sci.* **1977**, *255* (5), 468–479. https://doi.org/10.1007/BF01536463.
(7) Balakin, B. V; Hoffmann, A. C.; Kosinski, P. Experimental Study and Computational Fluid Dynamics Modeling of Deposition of Hydrate Particles in a Pipeline with Turbulent Water Flow. *Chem. Eng. Sci.* **2011**, *66* (4), 755–765. https://doi.org/10.1016/j.ces.2010.11.034.
(8) Balakin, B. V.; Lo, S.; Kosinski, P.; Hoffmann, A. C. Modelling Agglomeration and Deposition of Gas Hydrates in Industrial Pipelines with Combined CFD-PBM Technique. *Chem. Eng. Sci.* **2016**, *153*, 45–57. https://doi.org/10.1016/j.ces.2016.07.010.
(9) Balakin, B. V.; Hoffmann, A. C.; Kosinski, P. Population Balance Model for Nucleation, Growth, Aggregation, and Breakage of Hydrate Particles in Turbulent Flow. *AIChE J.* **2010**, *56* (8), 2052–2062. https://doi.org/10.1002/aic.12122.
(10) Sampaio, T. P.; Tavares, F. W.; Lage, P. L. C. Non-Isothermal Population Balance Model of the Formation and Dissociation of Gas Hydrates. *Chem. Eng. Sci.* **2017**, *163*, 234–254. https://doi.org/10.1016/j.ces.2016.12.012.
(11) Marchisio, D. L.; Pikturna, J. T.; Fox, R. O.; Vigil, R. D.; Barresi, A. A. Quadrature Method of Moments for Population-Balance Equations. *AIChE J.* **2003**, *49* (5), 1266–1276. https://doi.org/10.1002/aic.690490517.
(12) Marchisio, D. L.; Fox, R. O. Solution of Population Balance Equations Using the Direct Quadrature Method of Moments. *J. Aerosol Sci.* **2005**, *36* (1), 43–73. https://doi.org/10.1016/j.jaerosci.2004.07.009.
(13) Marchisio, D. L.; Vigil, R. D.; Fox, R. O. Quadrature Method of Moments for Aggregation–Breakage Processes. *J. Colloid Interface Sci.* **2003**, *258* (2), 322–334. https://doi.org/10.1016/S0021-9797(02)00054-1.
(14) Camargo, R. M. T. Propriétés Rhéologiques de Suspensions d'hydrate Dans Des Bruts Asphalténiques, PhD Thesis, Université Paris VI, Paris, France, 2001.
(15) Camargo, R.; Palermo, T. Rheological Properties of Hydrate Suspensions in an Asphaltenic Crude Oil. In *Proceedings of the Fourth International Conference on Gas Hydrates*; Yokohama, Japan, 2002; pp 880–885.
(16) Colombel, E. Cristallisation et Agglomération de Particules d'hydrate de Fréon Dans Une Émulsion Eau Dans Huile : Étude Expérimentale et Modélisation. PhD Thesis, Mines Saint-Etienne, Saint-Etienne, France, 2008.
(17) Colombel, E.; Gateau, P.; Barr'e, L.; Gruy, F.; Palermo, T. Discussion of Agglomeration

Mechanisms between Hydrate Particles in Water in Oil Emulsions. *Oil Gas Sci. Technol. - Rev. d'IFP Energies Nouv.* **2009**, *64* (5), 629–636. https://doi.org/10.2516ogst2009042.
(18) David, R.; Marchal, P.; Klein, J.-P.; Villermaux, J. Crystallization and Precipitation Engineering—III. A Discrete Formulation of the Agglomeration Rate of Crystals in a Crystallization Process. *Chem. Eng. Sci.* **1991**, *46* (1), 205–213. https://doi.org/https://doi.org/10.1016/0009-2509(91)80130-Q.
(19) Mumtaz, H. S.; Hounslow, M. J. Aggregation during Precipitation from Solution: An Experimental Investigation Using Poiseuille Flow. *Chem. Eng. Sci.* **2000**, *55* (23), 5671–5681. https://doi.org/https://doi.org/10.1016/S0009-2509(00)00202-5.
(20) Liew, T. L.; Barrick, J. P.; Hounslow, M. J. A Micro-Mechanical Model for the Rate of Aggregation during Precipitation from Solution. *Chem. Eng. Technol.* **2003**, *26* (3), 282–285. https://doi.org/10.1002/ceat.200390042.
(21) Cameirão, A. Etude Expérimentale et Modélisation d'une Précipitation Avec Agglomération Entre Cristaux de Morphologies Différentes : Application Au Molybdate de Strontium. PhD Thesis, Institut National Polytechnique de Toulouse, 2007.
(22) David, R.; Espitalier, F.; Cameirão, A.; Rouleau, L. Developments in the Understanding and Modeling of the Agglomeration of Suspended Crystals in Crystallization from Solutions. *KONA Powder Part. J.* **2003**, *21*, 40–53. https://doi.org/10.14356/kona.2003008.
(23) Cameirão, A.; Espitalier, F.; David, R.; Rouleau, L. Validation of a Model for Multiple Agglomeration. *Chem. Eng. Technol.* **2006**, *29* (2), 171–174. https://doi.org/10.1002/ceat.200500367.
(24) Smellie, R. H.; Mer, V. K. La. Flocculation, Subsidence and Filtration of Phosphate Slimes: VI. A Quantitative Theory of Filtration of Flocculated Suspensions. *J. Colloid Sci.* **1958**, *13* (6), 589–599. https://doi.org/https://doi.org/10.1016/0095-8522(58)90071-0.
(25) Thielmann, F.; Naderi, M.; Ansari, M. A.; Stepanek, F. The Effect of Primary Particle Surface Energy on Agglomeration Rate in Fluidised Bed Wet Granulation. *Powder Technol.* **2008**, *181* (2), 160–168. https://doi.org/10.1016/j.powtec.2006.12.015.
(26) Chua, K. W.; Makkawi, Y. T.; Hounslow, M. J. A Priori Prediction of Aggregation Efficiency and Rate Constant for Fluidized Bed Melt Granulation. *Chem. Eng. Sci.* **2013**, *98*, 291–297. https://doi.org/10.1016/j.ces.2013.05.018.
(27) Balakin, B. V; Kutsenko, K. V; Lavrukhin, A. A.; Kosinski, P. The Collision Efficiency of Liquid Bridge Agglomeration. *Chem. Eng. Sci.* **2015**, *137*, 590–600. https://doi.org/10.1016/j.ces.2015.07.002.
(28) Mills, P. Non-Newtonian Behaviour of Flocculated Suspensions. *J. Phys. Lettres* **1985**, *46* (7), 301–309. https://doi.org/10.1051/jphyslet:01985004607030100.
(29) Zerpa, L. E.; Sloan, E. D.; Sum, A. K.; Koh, C. A. Overview of CSMHyK: A Transient Hydrate Formation Model. *J. Pet. Sci. Eng.* **2012**, *98–99*, 122–129. https://doi.org/10.1016/J.PETROL.2012.08.017.
(30) Einstein, A. Eine Neue Bestimmung Der Moleküldimensionen. *Ann. Phys.* **1906**, *324* (2), 289–306. https://doi.org/10.1002/andp.19063240204.
(31) Einstein, A. Berichtigung Zu Meiner Arbeit: "Eine Neue Bestimmung Der Moleküldimensionen." *Ann. Phys.* **1911**, *339* (3), 591–592. https://doi.org/10.1002/andp.19113390313.
(32) Batchelor, G. K. The Stress System in a Suspension of Force-Free Particles. *J. Fluid Mech.* **1970**, *41* (3), 545–570. https://doi.org/DOI: 10.1017/S0022112070000745.
(33) Batchelor, G. K. The Effect of Brownian Motion on the Bulk Stress in a Suspension of

Spherical Particles. *J. Fluid Mech.* **1977**, *83* (1), 97–117. https://doi.org/10.1017/S0022112077001062.
(34) Batchelor, G. K.; Green, J. T. The Determination of the Bulk Stress in a Suspension of Spherical Particles to Order C2. *J. Fluid Mech.* **1972**, *56* (3), 401–427. https://doi.org/DOI: 10.1017/S0022112072002435.
(35) Macosko, C. *Rheology: Principles, Measurements, and Applications*, 1st ed.; Wiley-VCH, Ed.; Wiley-VCH, 1994.
(36) Guazzelli, É.; Morris, J. F. *A Physical Introduction to Suspension Dynamics*; 2011. https://doi.org/10.1017/CBO9780511894671.
(37) Krieger, I. M.; Dougherty, T. J. A Mechanism for Non-Newtonian Flow in Suspensions of Rigid Spheres. *Trans. Soc. Rheol.* **1959**, *3*, 137–152. https://doi.org/10.1122/1.548848.
(38) Bassani, C. L.; Barbuto, F. A. A.; Sum, A. K.; Morales, R. E. M. Modeling the Effects of Hydrate Wall Deposition on Slug Flow Hydrodynamics and Heat Transfer. *Appl. Therm. Eng.* **2017**, *114*, 245–254. https://doi.org/10.1016/j.applthermaleng.2016.11.175.
(39) Di Lorenzo, M.; Aman, Z. M.; Kozielski, K.; Norris, B. W. E.; Johns, M. L.; May, E. F. Modelling Hydrate Deposition and Sloughing in Gas-Dominant Pipelines. *J. Chem. Thermodyn.* **2018**, *117*, 81–90. https://doi.org/10.1016/j.jct.2017.08.038.
(40) Ramkrishna, D. *Population Balances: Theory and Applications to Particulate Systems in Engineering*, 1st ed.; San Diego, 2000.
(41) Yeoh, G. H.; Cheung, C. P.; Tu, J. *Multiphase Flow Analysis Using Population Balance Modeling: Bubbles, Drops and Particles*; Elsevier Inc.: Amsterdam, The Netherlands, 2014. https://doi.org/10.1016/C2011-0-05568-0.
(42) Kashchiev, D.; Firoozabadi, A. Nucleation of Gas Hydrates. *J. Cryst. Growth* **2002**, *243* (3–4), 476–489. https://doi.org/10.1016/S0022-0248(02)01576-2.
(43) Khurana, M.; Yin, Z.; Linga, P. A Review of Clathrate Hydrate Nucleation. *ACS Sustain. Chem. Eng.* **2017**, *5* (12), 11176–11203. https://doi.org/10.1021/acssuschemeng.7b03238.
(44) Warrier, P.; Khan, M. N.; Srivastava, V.; Maupin, C. M.; Koh, C. A. Overview: Nucleation of Clathrate Hydrates. *J. Chem. Phys.* **2016**, *145* (21), 211705. https://doi.org/10.1063/1.4968590.
(45) Melchuna, A. M.; Glenat, P.; Rivero, M.; Sum, A. K. Measurements of Dispersant Additive on Hydrate/Ice Slurry Transport. In *11th North American Conference on Multiphase Production Technology*; BHR Group: Banff, Canada, 2018; p BHR-2018-143.
(46) Kakitani, C.; Marques, D. C.; Neto, M. A. M.; Teixeira, A.; Valim, L. S.; Morales, R. E. M.; Sum, A. K. Dynamics of Hydrate Behavior in Shut-In and Restart Condition in Two and Three Phase System. *Offshore Technology Conference*. Offshore Technology Conference: Houston, Texas, USA 2020, p 8. https://doi.org/10.4043/30775-MS.
(47) Kakitani, C. Experimental Study of the Gas Hydrate Formation upon Shut-in and Restart of Gas and Oil Pipelines (in Portuguese), PhD Thesis, Federal University of Technology - Paraná, Curitiba, Brazil, 2019.
(48) Hinze, J. O. Fundamentals of the Hydrodynamic Mechanism of Splitting in Dispersion Processes. *AIChE J.* **1955**, *1* (3), 289–295. https://doi.org/10.1002/aic.690010303.
(49) Hughmark, G. A. Drop Breakup in Turbulent Pipe Flow. *AIChE J.* **1971**, *17* (4), 1000. https://doi.org/10.1002/aic.690170440.
(50) Kubie, J.; Gardner, G. C. Drop Sizes and Drop Dispersion in Straight Horizontal Tubes and in Helical Coils. *Chem. Eng. Sci.* **1977**, *32* (2), 195–202. https://doi.org/10.1016/0009-2509(77)80105-X.

(51) Brauner, N. The Prediction of Dispersed Flows Boundaries in Liquid-Liquid and Gas-Liquid Systems. *Int. J. Multiph. Flow* **2001**, *27* (5), 885–910. https://doi.org/10.1016/S0301-9322(00)00056-2.
(52) Espitalier, F.; David, R.; Schwartzentruber, J.; Baillon, F.; Gaunand, A.; Cournil, M.; Gruy, F.; Cameirão, A. Les Fondamentaux de la Cristallisation et de la Précipitation nte.mines-albi.fr/CristalGemme/co/CristalGemme.html (accessed Jan 25, 2018).
(53) Spielman, L. A. Viscous Interactions in Brownian Coagulation. *J. Colloid Interface Sci.* **1970**, *33* (4), 562–571. https://doi.org/10.1016/0021-9797(70)90008-1.
(54) Balakin, B.; Hoffmann, A. C.; Kosinski, P. The Collision Efficiency in a Shear Flow. *Chem. Eng. Sci.* **2012**, *68* (1), 305–312. https://doi.org/10.1016/j.ces.2011.09.042.
(55) Fuchs, N. Z. Über Die Stabilität Und Aufladung Der Aerosole. *Zeitschrift für Phys.* **1934**, *89* (11–12), 736–743. https://doi.org/10.1007/BF01341386.
(56) Bird, R. B.; Stewart, W. E.; Lightfoot, E. N. *Transport Phenomena*, 2nd ed.; John Wiley & Sons, 2002.
(57) Sander, R. Compilation of Henry's Law Constants (Version 4.0) for Water as Solvent. *Atmos. Chem. Phys.* **2015**, *15*, 4399–4981. https://doi.org/10.5194/acp-15-4399-2015.
(58) Lemmon, E. W.; Huber, M. L.; McLinden, M. O. REFPROP Reference Fluid Thermodynamic and Transport Properties. NIST Standard Reference Database 23 2013.
(59) Witherspoon, P. A.; Saraf, D. N. Diffusion of Methane, Ethane, Propane, and n-Butane in Water from 25 to 43°. *J. Phys. Chem.* **1965**, *69* (11), 3752–3755. https://doi.org/10.1021/j100895a017.
(60) Toolbox, T. E. The Engineering Toolbox. Diffusion coefficients of gases in water https://www.engineeringtoolbox.com/diffusion-coefficients-d_1404.html (accessed Sep 28, 2018).
(61) Dullien, F. A. L. *Porous Media: Fluid Transport and Pore Structure*, 1st ed.; Press, A., Ed.; Academic Press: New York, 1979.
(62) Carman, P. C. Fluid Flow through Granular Beds. *Trans. Inst. Chem. Eng.* **1937**, *15*, S32–S48. https://doi.org/10.1016/S0263-8762(97)80003-2.
(63) Ghanbarian, B.; Hunt, A. G.; Ewing, R. P.; Sahimi, M. Tortuosity in Porous Media: A Critical Review. *Soil Sci. Soc. Am. J.* **2013**, *77*, 1461–1477. https://doi.org/10.2136/sssaj2012.0435.
(64) KBC Products MultiflashTM: PVT Modelling and Flow Assurance Software https://www.kbc.global/uploads/files/services/KBC_Multiflash.pdf.
(65) Ballard, A. L.; Sloan, E. D. The next Generation of Hydrate Prediction: I. Hydrate Standard States and Incorporation of Spectroscopy. *Fluid Phase Equilib.* **2002**, *194–197*, 371–383. https://doi.org/10.1016/S0378-3812(01)00697-5.
(66) Jager, M. D.; Ballard, A. L.; Sloan, E. D. The next Generation of Hydrate Prediction: II. Dedicated Aqueous Phase Fugacity Model for Hydrate Prediction. *Fluid Phase Equilib.* **2003**, *211* (1), 85–107. https://doi.org/10.1016/S0378-3812(03)00155-9.
(67) Ballard, A. L.; Sloan, E. D. The next Generation of Hydrate Prediction: Part III. Gibbs Energy Minimization Formalism. *Fluid Phase Equilib.* **2004**, *218* (1), 15–31. https://doi.org/10.1016/j.fluid.2003.08.005.
(68) Ballard, A. L.; Sloan, E. D. The next Generation of Hydrate Prediction IV: A Comparison of Available Hydrate Prediction Programs. *Fluid Phase Equilib.* **2004**, *216* (2), 257–270. https://doi.org/10.1016/j.fluid.2003.11.004.
(69) Davies, J. T.; Rideal, E. K. *Interfacial Phenomena*, 1st ed.; Press, A., Ed.; Academic Press:

New York, 1961.
(70) Sigma-Aldrich. Arquad® 2HT-75 https://www.sigmaaldrich.com/catalog/product/aldrich/64402.
(71) Turner, D. J.; Miller, K. T.; Dendy Sloan, E. Methane Hydrate Formation and an Inward Growing Shell Model in Water-in-Oil Dispersions. *Chem. Eng. Sci.* **2009**, *64* (18), 3996–4004. https://doi.org/10.1016/j.ces.2009.05.051.
(72) Bassani, C. L.; Barbuto, F. A. A.; Sum, A. K.; Morales, R. E. M. A Three-Phase Solid-Liquid-Gas Slug Flow Mechanistic Model Coupling Hydrate Dispersion Formation with Heat and Mass Transfer. *Chem. Eng. Sci.* **2018**, *178*, 222–237. https://doi.org/10.1016/j.ces.2017.12.034.
(73) Fidel-Dufour, A.; Gruy, F.; Herri, J.-M. Rheology of Methane Hydrate Slurries during Their Crystallization in a Water in Dodecane Emulsion under Flowing. *Chem. Eng. Sci.* **2006**, *61* (2), 505–515. https://doi.org/https://doi.org/10.1016/j.ces.2005.07.001.
(74) Zerpa, L. E.; Rao, I.; Aman, Z. M.; Danielson, T. J.; Koh, C. A.; Sloan, E. D.; Sum, A. K. Multiphase Flow Modeling of Gas Hydrates with a Simple Hydrodynamic Slug Flow Model. *Chem. Eng. Sci.* **2013**, *99*, 298–304. https://doi.org/10.1016/j.ces.2013.06.016.
(75) Yan, K.-L.; Sun, C.-Y.; Chen, J.; Chen, L.-T.; Shen, D.-J.; Liu, B.; Jia, M.-L.; Niu, M.; Lv, Y.-N.; Li, N.; Song, Z.-Y.; Niu, S.-S.; Chen, G.-J. Flow Characteristics and Rheological Properties of Natural Gas Hydrate Slurry in the Presence of Anti-Agglomerant in a Flow Loop Apparatus. *Chem. Eng. Sci.* **2014**, *106*, 99–108. https://doi.org/https://doi.org/10.1016/j.ces.2013.11.015.

# Supporting Information of

# A Multiscale Approach for Gas Hydrates Considering Structure, Agglomeration, and Transportability under Multiphase Flow Conditions: III. Agglomeration Model

*Carlos L. Bassani*[†,‡], *Celina Kakitani*[‡], *Jean-Michel Herri*[†], *Amadeu K. Sum*[#*], *Rigoberto E.M. Morales*[‡*], *Ana Cameirão*[†*]

[†]Mines Saint-Etienne, Univ Lyon, CNRS, UMR 5307 LGF, Centre SPIN, Departement PEG, F - 42023 Saint-Etienne France

[‡]Multiphase Flow Research Center (NUEM), Federal University of Technology – Paraná (UTFPR), Rua Deputado Heitor Alencar Furtado, 5000, Bloco N, CEP 81280-340, Curitiba/PR, Brazil

[#]Phases to Flow Laboratory, Chemical and Biological Engineering Department, Colorado School of Mines, 1500 Illinois St., Golden, CO 80401, USA

This Supporting Information contains mathematical demonstrations and discussion on the validity of hypothesis adopted during the modeling of agglomeration of gas hydrate particles.

***<u>Demonstration #1</u>: finding the population balance written in the Method of Moments, eq. (6)***

Consider a closed control volume (CV) encompassing the liquid phase and let $f(L,t)$ be the size distribution of the particles per unit volume, given in [(particles/m$^3$)/m]. This size distribution varies in time due to the particles' growth, birth (nucleation, breakage) or death (agglomeration). A general expression for the population balance is

$$\underbrace{\frac{\partial}{\partial t}\int_{CV} d(\forall f)}_{\text{variation in time}} + \underbrace{\frac{\partial}{\partial L}\int_{CV} d(\forall G f)}_{\text{growth}} = \underbrace{\int_{CS} d(\forall h)}_{\text{birth and death}} \tag{S1}$$

where $L$ is the particle size, $G = \partial L/\partial t$ is the linear growth rate of the particles, and $h$ is the generation term of the balance equation, also known by birth and death terms. Considering that the control volume has a constant volume $\forall$, and that $G$ and $f$ are uniform inside the control volume, dividing by the volume $\forall$ and considering that the birth and death terms are composed by nucleation (*nuc*) and agglomeration (*agg*) of particles

$$\frac{\partial f}{\partial t} + \frac{\partial (Gf)}{\partial L} = h_{nuc} + h_{agg} \tag{S2}$$

being breakage out of the scope, since it is difficult to predict the amount of debris left by the particle breakage and their relative sizes. Multiplying by $L^j$ and integrating over the size range of the distribution (i.e., from 0 to infinite)

$$\underbrace{\int_0^\infty \frac{\partial f}{\partial t} L^j dL}_{(i)} + \underbrace{\int_0^\infty \frac{\partial (Gf)}{\partial L} L^j dL}_{(ii)} = \underbrace{\int_0^\infty h_{nuc} L^j dL}_{(iii)} + \underbrace{\int_0^\infty h_{agg} L^j dL}_{(iv)} \tag{S3}$$

where the moment of the particle size distribution, defined by $M_j = \int_0^\infty f L^j dL$, is easily recognized in term (i)

$$\int_0^\infty \frac{\partial f}{\partial t} L^j dL = \frac{\partial}{\partial t} \underbrace{\int_0^\infty f L^j dL}_{M_j} = \frac{\partial M_j}{\partial t} \tag{S4}$$

which represents the moment evolution in time. Term (ii) of eq (S3) represents the particle growth. Assuming that the linear growth rate $G$ has negligible variation with the particle size, $\partial G/\partial L \approx 0$, then

$$\int_0^\infty \frac{\partial (Gf)}{\partial L} L^j dL \approx G\int_0^\infty \frac{\partial f}{\partial L} L^j dL = \cancel{G\left[ f L^j \right]_0^\infty}^{=0} - G\int_0^\infty f \frac{\partial L^j}{\partial L} dL = -G\int_0^\infty f j L^{j-1} dL = -jGM_{j-1} \tag{S5}$$

where the regularity condition[1] should be noticed, $\lim_{L\to\infty}\left( f L^j \right) = 0$, which is interpreted as the inexistence of extremely large particles, i.e., when $L \to \text{large} \to \infty$, then $f \to 0$. Term (iii) of eq (S3) was already derived, eq (9) of the article, shown to be related to the initial condition of the population balance.

Term (iv) of eq (S3) represents the agglomeration of particles. Agglomeration is usually expressed in function of the density of particles in volume $f_v$. Therefore, $f_v dv$ represents the number of particles inside the particle volume interval $dv$. Considering that two particles with

volume $v_1$ and $v_2$ agglomerate forming a particle of volume $v = v_1 + v_2$ (hypothesis of no-porosity formation during agglomeration, although some interstitial liquid can be trapped inside the porous created during agglomeration, see Figure 4(e,f) of part I[2]), then the rate of agglomeration between these two particles is[3]

$$K_{agg(v_1,v_2)} f_{v(v_1)} f_{v(v_2)} dv_1 dv_2 \tag{S6}$$

where $K_{agg}$ is called the kernel of agglomeration. At the same time, the rate of particles of volume $v$ that vanish due to their agglomeration with particles of volume $v'$ is[1,3]

$$K_{agg(v',v)} f_{v(v')} f_{v(v)} dv' dv \tag{S7}$$

The total agglomeration rate $h_{agg}$ to form particles with volume $v$ is evaluated upon integrating eq (S6) over all particles from volume 0 to $v$ (divided by 2 so as to not count the interactions between $v_1$ and $v_2$ twice) minus the integration of eq (S7) upon all (0 to infinite) particles $v'$, therefore[3]

$$h_{agg} = \underbrace{\frac{1}{2}\int_0^v K_{agg(v_1,v_2)} f_{v(v_1)} f_{v(v_2)} dv_1 dv_2}_{\substack{\text{creation of particles with volume } v \text{ due to} \\ \text{agglomeration of particles with volume } v_1 \text{ and } v_2}} - \underbrace{f_{v(v)} dv \int_0^\infty K_{agg(v',v)} f_{v(v')} dv'}_{\substack{\text{vanishing of particles with volume } v \text{ due to} \\ \text{agglomeration of particle } v \text{ with } v'}} \tag{S8}$$

Since agglomeration uses the volume as variable of the distribution $f_v$, then the moment in volume must be defined

$$M_{vj} = \int_0^\infty f_v v^j dv \tag{S9}$$

Using eq (S8) for the total agglomeration rate $h_{agg}$, the equivalent of term (iv) of eq (S3) in volume comes

$$\dot{M}_{vj,agg} = \int_0^\infty h_{agg} v^j dv = \int_0^\infty \left[ \frac{1}{2}\int_0^v K_{agg(v_1,v_2)} f_{v(v_1)} f_{v(v_2)} dv_1 - f_{v(v)} \int_0^\infty K_{agg(v',v)} f_{v(v')} dv' \right] v^j dv \tag{S10}$$

By considering the kernel of agglomeration $K_{agg}$ to be independent of volumes $v_1, v_2$; by recognizing that $v = v_1 + v_2$, that is $v_1, v_2 < v$, meaning that the limit of integration in $v_1$ can be changed from $v$ to infinite; by recognizing that $v$ and $v'$ are independent; and by using the definition of the moment in volume of eq (S9); then eq (S10) comes

$$\dot{M}_{vj,agg} = \frac{K_{agg}}{2} \int_0^\infty \int_0^\infty \left(v_1 + v_2\right)^j f_{v(v_1)} f_{v(v_2)} dv_1 dv_2 - K_{agg} M_{vj} M_{v0} \tag{S11}$$

Eq (S11) represents the agglomeration contribution to the moments in volume. However, the population balance of eq (S3) if for the moments in size. The volume and the size of the particle are related by the volume factor as $v = \phi_v L^3$. The moment in volume therefore relates to the moment in size as

$$M_{vj} = \int_0^\infty f_{v(v)} v^j dv = \int_0^\infty f_{(L)} \left(\phi_v L^3\right)^j dL = \phi_v^j \underbrace{\int_0^\infty f_{(L)} L^{3j} dL}_{M_{3j}} = \phi_v^j M_{3j} \tag{S12}$$

By recognizing $f_{v(v)} dv = f_{(L)} dL$, that is, the number of particles in any representation (volume or size) is always the same, and by using the volume factor $\phi_v$ (which is independent of $L$ for a fixed particle geometry), the integrals of eq (S11) can be converted to size as

$$\dot{M}_{vj,agg} = \frac{K_{agg}}{2}\phi_v^j \int_0^\infty \int_0^\infty \left(L_1^3 + L_2^3\right)^j \, f_{(L_1)} f_{(L_2)} dL_1 dL_2 - K_{agg} M_{vj} M_{v0} \tag{S13}$$

By using the relation of eq (S12) and by recognizing that $M_{v0} = M_0 / \phi_v^0 = M_0$

$$\dot{M}_{3j,agg} = \frac{K_{agg}}{2}\int_0^\infty \int_0^\infty \left(L_1^3 + L_2^3\right)^j \, f_{(L_1)} f_{(L_2)} dL_1 dL_2 - K_{agg} M_{3j} M_0 \tag{S14}$$

and by transposing the index $j \leftarrow 3j$:

$$\dot{M}_{j,agg} = \frac{K_{agg}}{2}\int_0^\infty \int_0^\infty \left(L_1^3 + L_2^3\right)^{j/3} \, f_{(L_1)} f_{(L_2)} dL_1 dL_2 - K_{agg} M_j M_0 \tag{S15}$$

For $j = 0$, these integrals have analytical solution

$$\dot{M}_{0,agg} = \frac{K_{agg}}{2}\underbrace{\int_0^\infty f_{(L_1)} dL_1}_{M_0}\underbrace{\int_0^\infty f_{(L_2)} dL_2}_{M_0} - K_{agg} M_0 M_0 = -\frac{K_{agg}}{2} M_0^2 \tag{S16}$$

For the cases of $j \neq 3n$, with $n \in \mathbb{Z}$, eq (S15) does not have analytical solution, and a series expansion for term $\left(L_1^3 + L_2^3\right)^{j/3}$ is used[4]:

$$\left(L_1^3 + L_2^3\right)^{j/3} = \left(L_1^3\right)^{j/3} + \frac{1}{3} j L_2^3 \left(L_1^3\right)^{\frac{j}{3}-1} + \frac{\left(j-3\right) j L_2^6 \left(L_1^3\right)^{j/3}}{18 L_1^6} + \ldots \tag{S17}$$

Truncating for the first term, $\left(L_1^3 + L_2^3\right)^{j/3} \propto \left(L_1^3\right)^{j/3} = L_1^j$, introducing in eq (S15), considering a constant of proportionality $K_j$ due to the truncation, called agglomerate shape coefficient and considered to be independent of the size $L$ (more is discussed in demonstration #2), and solving the integral for $j = 1$

$$\dot{M}_{1,agg} = \frac{K_{agg}}{2} K_1' \underbrace{\int_0^\infty L_1 f_{(L_1)} dL_1}_{M_1}\underbrace{\int_0^\infty f_{(L_2)} dL_2}_{M_0} - K_{agg} M_1 M_0 = K_1 K_{agg} M_1 M_0 \tag{S18}$$

where $K_1$ absorbs the division by 2. For $j = 2$ and similar considerations

$$\dot{M}_{2,agg} = \frac{K_{agg}}{2} K_2' \underbrace{\int_0^\infty L_1^2 f_{(L_1)} dL_1}_{M_2}\underbrace{\int_0^\infty f_{(L_2)} dL_2}_{M_0} - K_{agg} M_2 M_0 = K_2 K_{agg} M_2 M_0 \tag{S19}$$

where $K_2$ absorbs the division by 2. For $j = 3$, the integrals of eq (S15) have analytical solution and the expansion in series is not necessary, thus

$$\dot{M}_{3,agg} = \frac{K_{agg}}{2}\left[\underbrace{\int_0^\infty L_1^3 f_{(L_1)} dL_1}_{M_3}\underbrace{\int_0^\infty f_{(L_2)} dL_2}_{M_0} + \underbrace{\int_0^\infty f_{(L_1)} dL_1}_{M_0}\underbrace{\int_0^\infty L_2^3 f_{(L_2)} dL_2}_{M_3}\right] - K_{agg} M_3 M_0 = 0 \tag{S20}$$

that is, agglomeration does not change the particle volume (per unit volume), which comes from the hypothesis of no porosity creation during agglomeration. Finally, eqs. (S4), (S5), and (S16) to (S20) are inserted in (S3) to find the population balance written in the Method of Moments for $j = [0,1,2,3]$

$$\begin{cases} \dfrac{dM_0}{dt} = -\dfrac{K_{agg}}{2} M_0^2 \\ \dfrac{dM_1}{dt} = GM_0 + K_1 K_{agg} M_1 M_0 \\ \dfrac{dM_2}{dt} = 2GM_1 + K_2 K_{agg} M_2 M_0 \\ \dfrac{dM_3}{dt} = 3GM_2 \end{cases} \tag{S21}$$

which is eq (6) of the article.

***Demonstration #2*: determination of the agglomerate shape coefficients $K_1, K_2$**

Due to the lack of proper instrumentation to measure the particle size distribution, the parameters $K_1, K_2$ of eq (6) cannot be regressed experimentally. The values of Herri et al.[5] were adopted, being $K_1 = -0.262$ and $K_2 = -0.113$. Here, we demonstrate the meaning of those parameters, and that the adopted values have a plausible order of magnitude even when extending the scenario to systems containing oil. Figure S1a presents the case of two spheres of radius $r_1, r_2$ that form a spherical agglomerate of radius $r$. Considering that no porosity is created during agglomeration, the final agglomerate radius come

$$v = v_1 + v_2 \therefore r^3 = r_1^3 + r_2^3 \therefore r = r_1 \left[ 1 + \left( \frac{r_2}{r_1} \right)^3 \right]^{1/3} \tag{S22}$$

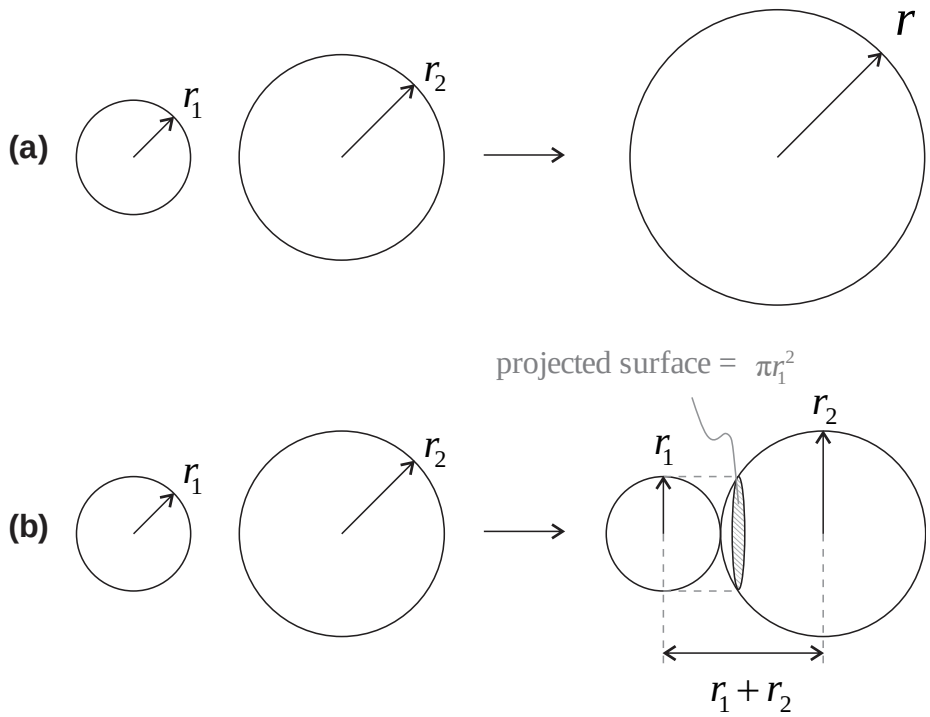


Figure S1. Geometric assumption of agglomerate shape: (a) sphere, and (b) sticked-spheres.

By considering the agglomeration of two isolated particles (but not the entire particle population), the contribution of agglomeration to the moment in size of 1st and 2nd order, eqs (S18) and (S19), are simplified to $M_{j,agg} \approx K_j M_j$, since term $K_{agg} M_0$ comes at play when dealing with the entire particle population, the probability of collision, and the agglomeration efficiency. Notice as well that the dot over $M_{j,agg}$ is not used anymore, since this dot represents the variation in time of the moment $M_j$ due to agglomeration (agg). The time dependence is inside the term $K_{agg} M_0$, with units [$s^{-1}$], which is not important when the interest is in two isolated particles. That is, the problem is purely geometric. Furthermore, for two isolated particles, the concept of moment of particle size distribution does not exist, and instead the physical parameters (length, surface) are used. For $j=1$, parameter $K_1$ is given by the variation of the total particle length before and after agglomeration, $M_{1,agg} \approx r-(r_1+r_2)$, divided by the final length, $M_1 \approx r$

$$K_1 \approx \frac{M_{1,agg}}{M_1} \approx \frac{r-(r_1+r_2)}{r} = 1 - \frac{\frac{r_1}{r_2}+1}{\frac{r_1}{r_2}\left[1+\left(\frac{r_2}{r_1}\right)^3\right]^{1/3}} \tag{S23}$$

For $j=2$, parameter $K_2$ is given by the variation of the particle surface before and after agglomeration, $M_{2,agg} \approx 4\pi\left(r^2 - r_1^2 - r_2^2\right)$, divided by the final outer surface, $M_2 \approx 4\pi r^2$

$$K_2 \approx \frac{M_{2,agg}}{M_2} \approx \frac{4\pi\left(r^2 - r_1^2 - r_2^2\right)}{4\pi r^2} = 1 - \frac{\left(\frac{r_1}{r_2}\right)^2+1}{\left(\frac{r_1}{r_2}\right)^2\left[1+\left(\frac{r_2}{r_1}\right)^3\right]^{2/3}} \tag{S24}$$

A more realistic agglomerate shape is the case of two sticked-spheres (*doublet*), as presented in Figure S1b. In this case, however, there is not a unique length that describe the agglomerate. Let the equivalent size $r$ of the agglomerate be the average of the three characteristic lengths of the agglomerate, namely $r_1$, $r_2$ and $r_1+r_2$, then

$$r = \frac{r_1+r_2+(r_1+r_2)}{3} = \frac{2}{3} r_1\left(1+\frac{r_2}{r_1}\right) \tag{S25}$$

For $j=1$

$$K_1 \approx \frac{M_{1,agg}}{M_1} \approx \frac{r-(r_1+r_2)}{r} = -\frac{1}{2} \tag{S26}$$

but if the maximum length $r_1+r_2$ of the agglomerate is used instead of the averaged one, then

$$K_1 \approx \frac{M_{1,agg}}{M_1} \approx \frac{r-r_1-r_2}{r} = 0 \tag{S27}$$

Eq (S26) and (S27) are approximations, and $K_1$ considering this agglomerate shape is something in between $0 < -K_1 < 0.5$. For $j=2$, it is considered that the surface in contact with

the continuous phase, which vanishes after agglomeration, is the projection of the smaller sphere, $\pi r_1^2$ for $r_1/r_2 < 1$, multiplied by 2 since this surface vanishes in both particles

$$K_2 \approx \frac{M_{2,agg}}{M_2} \approx \frac{\left[4\pi\left(r_1^2+r_2^2\right)-2\pi r_1^2\right]-4\pi\left(r_1^2+r_2^2\right)}{\left[4\pi\left(r_1^2+r_2^2\right)-2\pi r_1^2\right]} = -\frac{\left(\frac{r_1}{r_2}\right)^2}{\left(\frac{r_1}{r_2}\right)^2+2} \tag{S28}$$

Figure S2 shows plots of $K_1, K_2$ using both geometrical models, the sphere and the sticked-sphere agglomerate, for the range of $0 \le r_1/r_2 \le 1$ (notice that, e.g., $r_1/r_2 = 10$ is equivalent to $r_1/r_2 = 0.1$, since what matters is the proportion between the agglomerating particles). The geometric models converge to the ranges of $0 \le -K_1 < 0.6$ and $0 \le -K_2 \le 0.\overline{3}$, always present negative values, and always give $K_1/K_2 > 0$. Therefore, the values regressed by Herri et al.[5] are physically acceptable. It is important to notice that $K_1, K_2 = f\left(r_1/r_2\right)$ and that the Method of Moments has no information about the ratio of the size of the particles prior to agglomeration. Therefore, $K_1, K_2$ need to assume a unique value that is representative for the entire agglomeration process and that is independent of $r_1, r_2$. This is an approximation of the Method of Moments which can be avoided by the use of more sophisticated mathematical approaches to solve the population balance, at however higher computational cost.

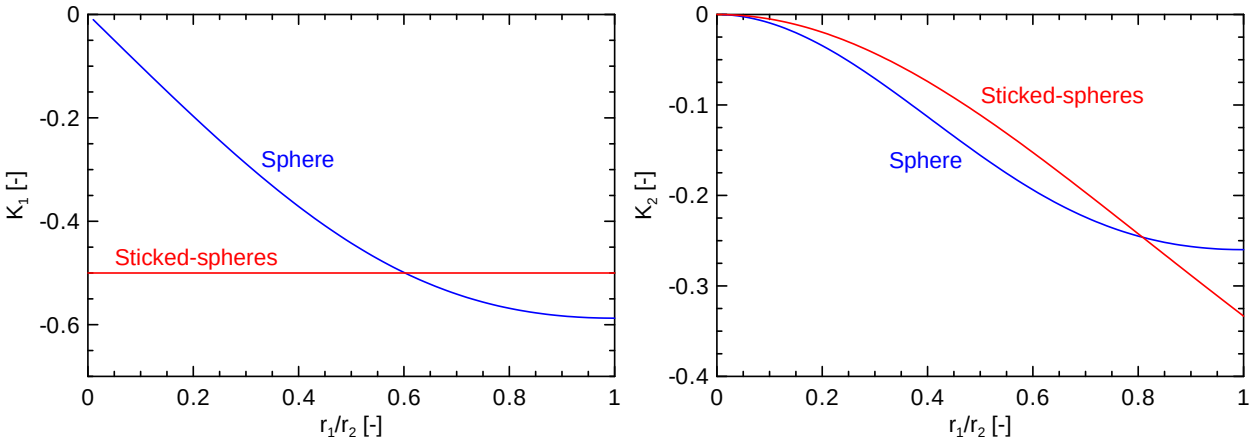


Figure S2. Evaluation of the theoretical agglomerate shape coefficients (a) $K_1$ and (b) $K_2$ against the ratio of the agglomerating particle radii $r_1/r_2$ considering the sphere and the sticked-sphere geometrical models for the agglomerate.

***Demonstration #3*: Smoluchowski's collision rate and its applicability to the analyzed system**

Consider a particle with radius $r_1$ at a reference position $x = 0$ with velocity $u|_{x=0}$ flowing at its streamline, as depicted in Figure S3. A second particle of radius $r_2$ is flowing in a different

streamline at a velocity $u_{(x)} = \left(\frac{du}{dx}\right)x + u\big|_{x=0}$, $\dot{\gamma} = \frac{du}{dx} = cte$ being a constant shear rate. If the streamline of the second particle is in a distance equal or smaller than the distance for contact between the two particles (that is, $R_{12} = r_1 + r_2$ when considering no long-range interaction between particles), then the particle $r_2$ will approach and collide with particle $r_1$ due to the relative velocity $u_{(x)} - u\big|_{x=0} = \left(\frac{du}{dx}\right)x = \dot{\gamma} z$. The rate of collision between these two particles is given by the flux of particles $r_2$ crossing a circular section of radius $R_{12}$

$$J = \int_{-R_{12}}^{R_{12}} \left[ u_{(x)} - u\big|_{x=0} \right] dA \tag{S29}$$

By recognizing the element of area of a circle in Cartesian coordinates as $dA = \left(2\sqrt{R_{12}^2 - z^2}\right)dz$, and that the integration can be done for a semicircle and multiplied by 2, that is, $\int_{-R_{12}}^{R_{12}} ... = 2\int_{0}^{R_{12}} ...$, and by using the relative velocity for $\dot{\gamma} = cte$, then:

$$J = 2\int_0^{R_{12}} \dot{\gamma} z \left(2\sqrt{R_{12}^2 - z^2}\right) dz = 4\dot{\gamma} \underbrace{\int_0^{R_{12}} z\sqrt{R_{12}^2 - z^2}\, dz}_{R_{12}^3/3} = \frac{4}{3}\dot{\gamma} R_{12}^3 = \frac{4}{3}\dot{\gamma}\left(r_1 + r_2\right)^3 \tag{S30}$$

Considering a population of $n_1$ particles (per unit volume) with radius of $r_1$, and $n_2$ particles (per unit volume) with radius of $r_2$, the total collision rate comes

$$J = \frac{4}{3}\dot{\gamma}\left(r_1 + r_2\right)^3 n_1 n_2 \tag{S31}$$

and by comparing with the general expression of agglomeration/collision rate, given by $k n_1 n_2$, the rate of collision comes

$$k_{col} = \frac{4}{3}\dot{\gamma}\left(r_1 + r_2\right)^3 \tag{S32}$$

or yet by considering an averaged particle size, $r_1 = r_2 = r_p$, then

$$k_{col} \approx \frac{32}{3}\dot{\gamma} r_p^3 = \frac{32}{3}\dot{\gamma}\left(\frac{M_1}{M_0}\right)^3 \tag{S33}$$

where the moments of particle size are used to express the particle average radius. This is eq (11) of the article. Notice that, beside neglecting long-range interactions, the sole hypothesis is the existence of a constant shear rate, which is however rarely found in practice. The flow in the bulk of the adopted rock-flow cell is turbulent, and therefore it is not expected that this collision rate holds perfectly. The consideration of turbulent collision rate expression implies, however, into the determination of the turbulent field, which is of a much higher complexity and computational cost than the model proposed in this article. *Smoluchowski's collision rate is therefore considered to hold, at least in its trends of proportionality with the shear rate and the average particle radius to the third order, when considering an averaged order of magnitude of the shear rate*. In demonstration #5, it is shown that, far from the wall (that is, in the liquid bulk, where agglomeration is mostly happening), the shear rate remains in the same order of magnitude and, therefore, can be approximated by a constant averaged value.

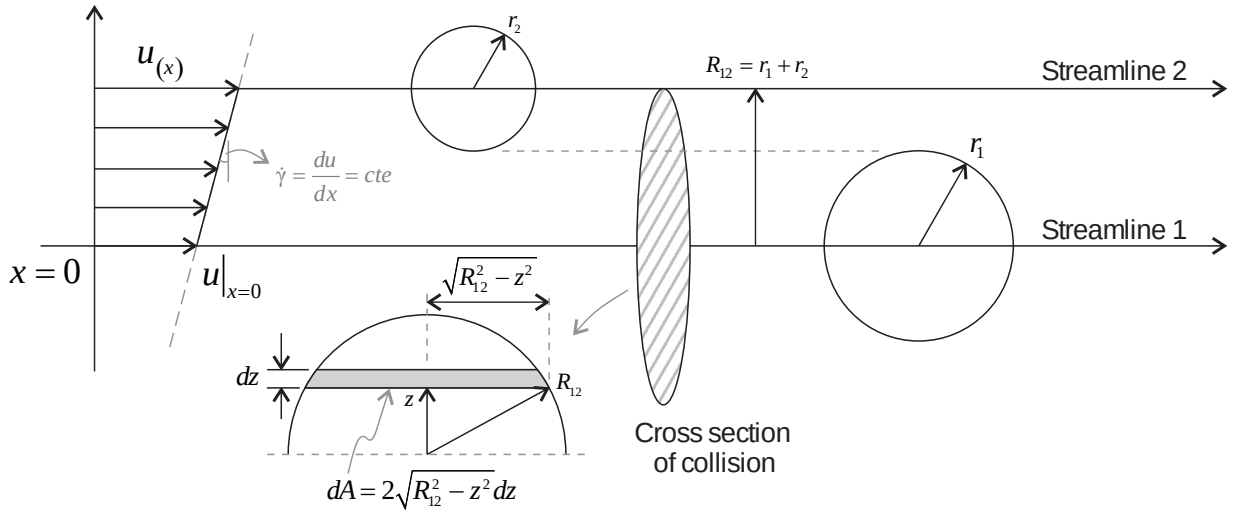


Figure S3. Depiction of two colliding particles in order to predict the collision rate when shear rate is constant and for negligible long-range particle interaction.

***Demonstration #4*: coupling the growth kinetics model of part II with the moments of particle size distribution**

In part II[2], the aim was to model the gas consumption rate of hydrate formation based on the mass transfer of a spherical particle of radius and outer surface $4\pi r_p^2$, and to multiply the results by the $n_p$ particles of the system. In part III, we extend the concept to a population of particles described by the statistic parameter called the moments of particle size distribution $M_j$. Therefore, in the growth kinetics equations, the terms related to the particle-bulk interface shall be computed as $4\pi r_p^2 \approx M_2/M_0$ for a single particle, and $4\pi r_p^2 n_p \approx M_2 \forall_L$ for the entire particle population, where the use of the second moment $M_2$ does not necessarily implies in a spherical agglomerate, but depends on the agglomerate shape coefficients $K_j$ adopted to solve the population balance of eq (6). Therefore, the following equations of part II[2] are changed of representation: eq (11) for the gas consumption rate in the outer surface of one particle, eqs (23) and (24) for the growth rate inside all capillaries of one particle, eq (31) to transform the number of capillaries into porosity, and eq (33) for the total consumption of gas due to hydrate formation. These equations come, respectively

$$-\left.\frac{dn_{g,i}}{dt}\right|_{out} = \min\left\{\begin{array}{l} \dfrac{\zeta}{12}\dfrac{\rho_w}{\eta M_w}\dfrac{r_c}{\tau^2}\dfrac{\sigma_{o/w}\cos\theta_{o/w/h}}{\mu_w}\dfrac{M_2}{M_1}\varepsilon \quad ; \\ \dfrac{M_2}{M_0}\dfrac{k_i}{H_o}\left[C_b - H_o f_{eq} - \dfrac{M_0}{M_2}\dfrac{1}{h_{m,p/b}}\left(-\left.\dfrac{dn_{g,i}}{dt}\right|_{hyd}\right)\right] \end{array}\right\} \tag{S34}$$

$$-\left.\frac{dn_{g,i}}{dt}\right|_{cap} = n_c \frac{\pi r_c^{3/2}}{(1+\omega)}\sqrt{2H_w D_w k_i}\left[\frac{C_b}{H_o} - f_{eq} - \frac{M_0}{M_2}\frac{1}{H_o h_{m,p/b}}\left(-\left.\frac{dn_{g,i}}{dt}\right|_{out}\right)\right] \tag{S35}$$

$$\omega = \frac{\pi n_c r_c^{3/2}}{h_{m,p/b}}\frac{H_w}{H_o}\frac{M_0}{M_2}\sqrt{\frac{2D_w k_i}{H_w}} \tag{S36}$$

$$\varepsilon = \pi n_c r_c^2 \frac{M_0}{M_2} \tag{S37}$$

$$-\left.\frac{dn_g}{dt}\right|_{hyd} = M_0 \forall \left( -\left.\frac{dn_{g,i}}{dt}\right|_{out} - \left.\frac{dn_{g,i}}{dt}\right|_{cap} \right) \tag{S38}$$

The nomenclature and physics associated to these equations were already presented in part II[2].

***Demonstration #5*: determination of the shear rate in the rock-flow cell, and determination of $k_{Kolm}$**

The shear rate is an important parameter for the estimation of the collision rate, eq (11), and for the disruption rate, eq (23) of the article. It is however not a simple task to retrieve its value, and often Computational Fluid Dynamics (CFD) is required and gives good results for the velocity field, but not necessarily for the shear rate, being very sensitive to the mesh adopted. Here, we seek a simple way to estimate the order of magnitude of the shear rate in means of the mixture velocity $U$. For such a purpose, we consider that the velocity profile inside the rock-flow cell can be estimated by a turbulent model considering single-phase, steady-state, developed flow in a smooth pipe as (see section 1.7 of Ghiaasiaan[6])

$$u^+ = \begin{cases} y^+, \;\; y^+ < 5 \\ 5\ln y^+ - 3.05, \;\; 5 < y^+ < 30 \\ 2.5\ln y^+ + 5.5, \;\; 30 < y^+ \le 400 \end{cases} \tag{S39}$$

where the shear rate comes from the derivation of eq (S39)

$$\dot{\gamma}^+ = \frac{du^+}{dy^+} = \begin{cases} 1, \;\; y^+ < 5 \\ \dfrac{5}{y^+}, \;\; 5 < y^+ < 30 \\ \dfrac{2.5}{y^+}, \;\; 30 < y^+ \le 400 \end{cases} \tag{S40}$$

and the dimensionless variables are $y^+ = \frac{yU_\tau}{\nu}$, $u^+ = \frac{u}{U_\tau}$, $\dot{\gamma}^+ = \frac{\nu}{U_\tau^2}\dot{\gamma}$ and $U_\tau = \sqrt{\tau_w/\rho}$ and the expression used for the shear stress at the wall comes from Blasius (smooth pipe), $\tau_w = 0.0332\rho U^2 \left(\frac{\nu}{RU}\right)^{0.25}$, being $R$ the radius and $\nu$ the kinematic viscosity (of the continuous phase, that is, the oil, thus $\nu_o = \mu_o/\rho_o$). Eq (S40) depends on the distance to the wall $y$, and on the oil viscosity, which is an open-question at the pressurized conditions as discussed in section 3.

Figure S4a shows the shear rate $\dot{\gamma}$ against the distance to the wall $y$ for a density of $\rho_o = 850$ kg/m$^3$ and for different oil viscosities in the range of $1 \le \mu_o \le 40$ cP, considered to be plausible for the oil at 70 bar, and considering a velocity of $U = 0.26$ m/s (relative to 16 rpm of the rock-flow cell oscillation rate). Plots are given for $0 \le y \le 25$ mm, since the diameter of the rock-flow cell is 50.8 mm and the related liquid loading is 50%. Notice that, since the flow is not in a circular section, then the radius $R$ is half of the hydraulic diameter. However, by

considering that the liquid occupies 50% of the cross section (due to 50% of liquid loading) and that the cross section geometry is half of a circle, than the hydraulic diameter is the same as the rock-flow cell diameter, that is, $R = 25.4\,\text{mm}$. From Figure S4a, it is noticeable the fact that: (i) for low viscosities ($\leq 5$ cP), the shear rate close to the wall is in the order of magnitude of ~ 50-250 $s^{-1}$, but the flow quickly transitions to the inertial sublayer $(y^+ > 30)$, and the shear rate drops to an order of magnitude of 1-20 $s^{-1}$ a few millimeters far from the wall, and (ii) for higher viscosities (> 5 cP), the shear rate remains in the order of magnitude of 1-50 $s^{-1}$ close to the wall, and also reaches the range of 1-20 $s^{-1}$ a few millimeters away from it. Figure S4b shows the shear rate against the oil viscosity plotted in the wall $(y = 0)$ and at distances of 10 and 20 mm of the wall. The only large difference for the different oil viscosities held to the of order of magnitude of the shear rate is for flow close to the wall. Since agglomeration is considered to happen in the liquid bulk, then the order of magnitude of 1-20 $s^{-1}$ can be considered to represent the average shear rate $\dot{\gamma}$ for the agglomeration model.

In this article, an average of the values of shear rates evaluated at 10, 15 and 20 mm from the wall is used, leading to the values of Table 3 of the article. It is important to notice that the velocity in the rock-flow cell is not known a priori, but a velocity-scale can be retrieved. The oscillation rate $\omega = [6, 11.25, 16]$ rpm of Kakitani et al.[7,8] is reported for the complete cycle of the rock-flow cell, that is, for an downward and upward movement, where the liquid flows from one side to another of the rock-flow cell, with length $L$, and comes back to its initial position. That is, the total displacement is $2L$. The time scale is the inverse of the oscillation rate, $\Delta t = \omega^{-1}$ (given in minutes if $\omega$ is in rpm, or in seconds if $\omega$ is in Hz), and therefore the velocity scale is $U \propto \dfrac{2L}{\Delta t} = 2\omega L$.

However, the intermediary step of calculating the shear rate by an $u^+(y^+)$ velocity profile, as the one presented in eq (S39), is not desirable for quick engineering applications, that is, when a simplified model is sought. Considering a fluid element, the net force $F = \Delta P \cdot A$ is due to the application of a pressure difference $\Delta P = \dfrac{dP}{dz} L$ in the direction of the flow $z$, where $A$ is the cross section of the pipeline and $L$ its length, and $\forall = AL$ is the pipeline volume. The work is the force multiplied by the displacement, and per unit time held the power, $\dot{E} = \dfrac{E}{\Delta t} = \dfrac{F \Delta x}{\Delta t} = FU = U \dfrac{dP}{dL} \forall$. The energy dissipation rate $\varepsilon_t$ is the power per unit mass $m = \rho \forall$, thus

$$\varepsilon_t = \frac{U}{\rho} \frac{dP}{dL} = \frac{2 f U^3}{D} \tag{S41}$$

where the pressure gradient comes from the friction factor in Fanning representation as $\dfrac{dP}{dL} = 2\rho \dfrac{f U^2}{D}$. That is, by the knowledge of the mixture velocity, and by adopting a friction factor correlation (which implies in the same hypothesis of adopting the correlation of the shear stress in the wall $\tau_w$ by the $u^+(y^+)$ approach), one can find the energy dissipation rate. From the 1st similarity hypothesis of Kolmogorov, in every turbulent flow at sufficiently high Reynolds number, the statistics of the small scale motions (in the Kolmogorov scale) have a universal form

that is uniquely determined by the energy dissipation rate $\varepsilon_t$ and by the kinematic viscosity $\nu$. From dimensionless analysis, the shear rate therefore relates to the energy dissipation rate as

$$\dot{\gamma} \propto \sqrt{\frac{\varepsilon_t}{\nu}} \tag{S42}$$

where a constant of proportionality of $k_{Kolm} \approx 1$ is often adopted in literature (that is, that this relation is actually an equality). By comparing the analytic solution of Poiseuille flow (laminar flow in a pipeline induced by pressure difference, where the average shear rate is $\bar{\dot{\gamma}} = \int \frac{r}{2\mu}\frac{\partial P}{\partial x} dA = \frac{R}{3\mu}\frac{\partial P}{\partial x}$) with eq (S42), one finds $k_{Kolm} \approx 0.94$. Eq (S42) can as well be compared to the shear rate at the wall by using the eq (S40) at $y = 0$, which leads to $0.2 \le k_{Kolm} \le 3.3$ when considering the oil density of $\rho_o = 850$ kg/m$^3$, the oil viscosity in the range of $1 \le \mu_o \le 40$ cP and the geometry of the rock-flow cell ($R = 25.4$ mm and $0.1 \le U \le 0.26$ m/s). That is, eq (S42) already escapes a bit the values for the wall shear rate. But, as said, the agglomeration occurs mainly in the liquid bulk, where the flow is in the inertial sublayer (the flow is turbulent), and the 1st similarity of Kolmogorov is not valid. By estimating the average shear rate at positions 10, 15 and 20 mm from the wall for a 10 cP oil viscosity, and by considering the rock-flow cell geometry $D = 50.8$ mm and the velocities in the range of $0.1 \le U \le 0.26$ m/s, one finds $k_{Kolm} \approx -1.25\omega + 0.57$. Or yet, for the purpose of estimating parameters $k_5 - k_7$ of the simplified agglomeration model, one can adopt $k_{Kolm} \approx 0.23$. This value uniquely holds for the dataset tested, thence $k_5 - k_7$, eqs (39) to (41) of the article, are probably apparatus-dependent. An engineering-alternative is to experimentally regress parameters $k_5 - k_7$ for each dataset of interest in order to avoid estimation of $k_{Kolm}$ for each system tested. This experimental regression will absorb any ill-posed hypothesis of this demonstration and is the unique way to assure precision of the model, unless enhanced knowledge of the turbulent field is available.

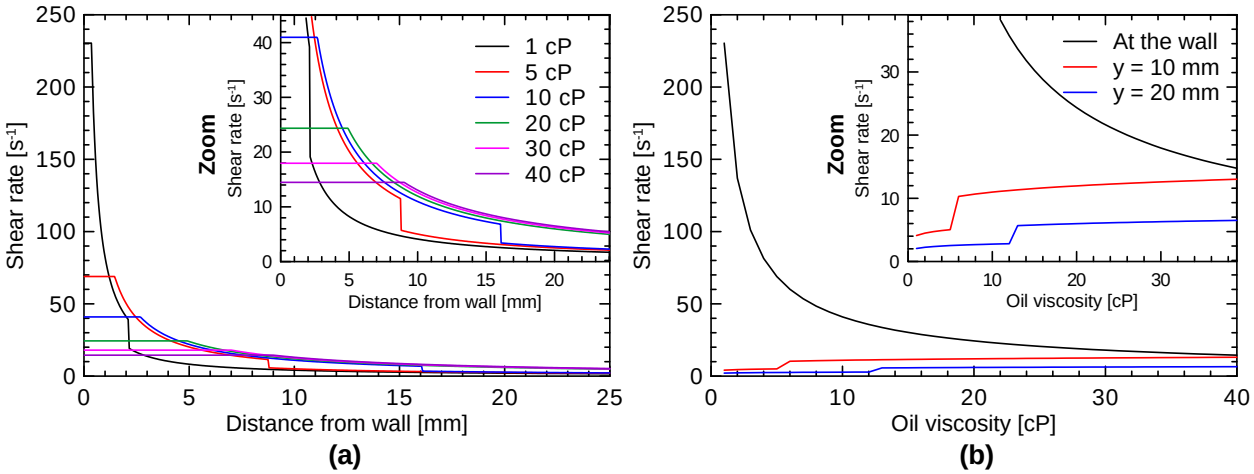


Figure S4. (a) Shear rate against the distance from the wall for different oil viscosities. (b) Shear rate against viscosity plotted for different distances from the wall.

***Demonstration #6:*** **proof of the hypothesis that representative values of the moment of particle size distribution exist**

The major simplifying hypothesis in section 5 is the existence of representative values of the moment of particle size distribution $\bar{M}_j$ that hold for the entire agglomeration process and that are able to represent the dataset tested. The values $\frac{\bar{M}_0}{\bar{M}_1} \approx 100\ \text{m}^{-1}$, $\frac{\bar{M}_1^4}{\bar{M}_0^3} \approx 1\times10^{-4}$ m and $\frac{\bar{M}_3}{\bar{M}_2^2} \approx 9\times10^{-6}\ \text{m}^2$ were adopted to retrieve $k_3 - k_7$ from their theoretical expressions, eqs (37) to (41) of the article, and hold as representative values. From the complete model, the moments stay inside the ranges $80 \le \frac{\bar{M}_0}{\bar{M}_1} \le 900\ \text{m}^{-1}$, $2.9\times10^{-5} \le \frac{\bar{M}_1^4}{\bar{M}_0^3} \le 3.4\times10^{-3}$ m and $1.2\times10^{-6} \le \frac{\bar{M}_3}{\bar{M}_2^2} \approx 2.3\times10^{-5}\ \text{m}^2$, and therefore the simplifying hypothesis is valid for, at least, the dataset tested.

***Demonstration #7:*** **finding the simplified expression for the particle / agglomerate radius evolution in time $r_{p(t)}$, eq (28)**

The population balance expressed in the Method of Moments, eq (6) of the article, is simplified to the 0th and 1st orders only, since the focus is on determining the size, and to the agglomeration process only, which is related to more pronounced variations in size that growth. Therefore

$$\begin{cases} \dfrac{dM_0}{dt} = -\dfrac{K_{agg}}{2} M_0^2 \\ \dfrac{dM_1}{dt} = K_1 K_{agg} M_1 M_0 \end{cases} \tag{S43}$$

The variation rate of the average particle radius comes from deriving its definition

$$r_p = \frac{M_1}{M_0} \quad \therefore \quad \frac{dr_p}{dt} = \frac{d}{dt}\left(\frac{M_1}{M_0}\right) = \frac{1}{M_0}\frac{dM_1}{dt} - \frac{M_1}{M_0^2}\frac{dM_0}{dt} \tag{S44}$$

and by using eq (S43) comes

$$\frac{dr_p}{dt} = \left(\frac{1}{2} + K_1\right) M_1 K_{agg} \tag{S45}$$

Calling $a_1 = \left(\frac{1}{2} + K_1\right)\bar{M}_1$, recognizing that $a_1 K_{agg} \approx cte$ since the increase in particle size from Figure 7 of the article is fairly linear, and integrating in time

$$r_p = r_{p,in} + a_1 K_{agg} t \tag{S46}$$

which is eq (28) of the article.

***Demonstration #8:*** **sigmoid function for the porous media interconnectivity, eq (34)**

The sigmoid function for the porous media interconnectivity, eq (33) of the article, was chosen since it predicts the two asymptotes. Figure S5 shows plots of the sigmoid function for a fixed $\Delta T^* = 15$ K and different $a_6$ values. The values of $a_6 = 1\,\text{K}^{-1}, \Delta T^* = 15$ K are adopted for the

model, but a refined dataset for the subcooling, if ever available, would be more accurate values of those parameters. Parameter $a_6$ dictates how fast is the variation from the maximum to the minimum plateau, whereas $\Delta T^*$ dictates the subcooling at which the lower interconnectivity plateau is reached. For a matter of comparison, an exponential function is plotted (dashed line) in Figure S5, given by $\zeta_{(\Delta T)} = 19.7\Delta T^{-3.42}$. The exponential function is usually the first function to be adopted when a decaying, asymptotic trend is required, and it presents similar results to the sigmoid with $a_6 = 0.7 - 1\,\mathrm{K}^{-1}$ in the range of $7.5 \le \Delta T \le 18\,\mathrm{K}$. However, it is noticeable that the extrapolation of this exponential function for $\Delta T < 7.5$ cause unrealistic values of $\zeta >> 0.02$, leading to very high $t_{dry}$. In order to limit the range of $0.001 \le \zeta \le 0.02$, the sigmoid function was adopted.

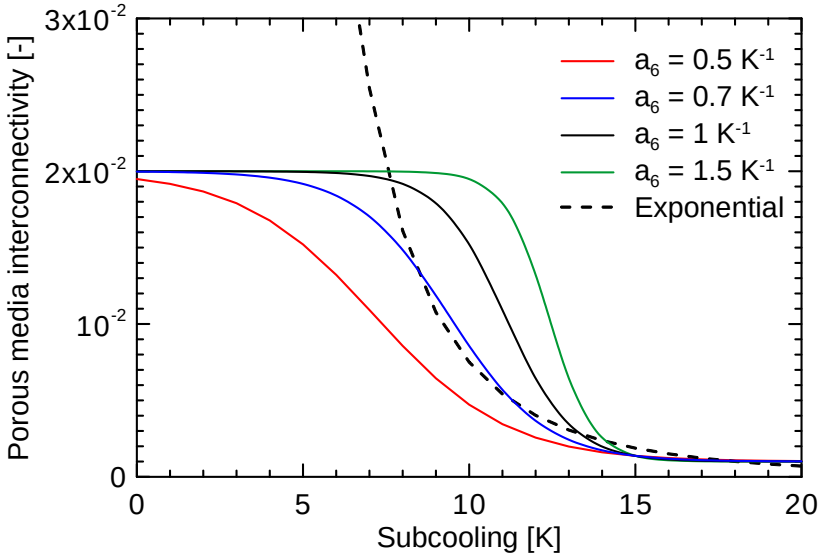


Figure S5. Porous media interconnectivity for the sigmoid function (continuous lines) for different $a_6$ values, compared to an exponential regression (dashed line).

**Additional References**


(1) Ramkrishna, D. *Population Balances: Theory and Applications to Particulate Systems in Engineering*, 1st ed.; San Diego, 2000.

(2) Bassani, C. L.; Sum, A. K.; Herri, J.-M.; Morales, R. E. M.; Cameirão, A. A Multiscale Approach for Gas Hydrates Considering Structure, Agglomeration, and Transportability under Multiphase Flow Conditions: II. Growth Kinetic Model. *Ind. Eng. Chem. Res.* **2020**, *59* (5), 2123–2144. https://doi.org/10.1021/acs.iecr.9b04245.

(3) Espitalier, F.; David, R.; Schwartzentruber, J.; Baillon, F.; Gaunand, A.; Cournil, M.; Gruy, F.; Cameirão, A. Les Fondamentaux de la Cristallisation et de la Précipitation nte.mines-albi.fr/CristalGemme/co/CristalGemme.html (accessed Jan 25, 2018).

(4) Wolfram Alpha LLC. Wolfram|Alpha. 2009.

(5) Herri, J. M.; Pic, J. S.; Gruy, F.; Cournil, M. Methane Hydrate Crystallization Mechanism from In-Situ Particle Sizing. *AIChE J.* **1999**, *45* (3), 590–602. https://doi.org/10.1002/aic.690450316.

(6) Mostafa Ghiaasiaan, S. *Two-Phase Flow, Boiling and Condensation: In Conventional and*

*Miniature Systems*, 1st ed.; Press, C. U., Ed.; Cambridge University Press, 2008. https://doi.org/10.1017/CBO9780511619410.
(7) Kakitani, C. Experimental Study of the Gas Hydrate Formation upon Shut-in and Restart of Gas and Oil Pipelines (in Portuguese), PhD Thesis, Federal University of Technology - Paraná, Curitiba, Brazil, 2019.
(8) Kakitani, C.; Marques, D. C.; Neto, M. A. M.; Teixeira, A.; Valim, L. S.; Morales, R. E. M.; Sum, A. K. Dynamics of Hydrate Behavior in Shut-In and Restart Condition in Two and Three Phase System. *Offshore Technology Conference*. Offshore Technology Conference: Houston, Texas, USA 2020, p 8. https://doi.org/10.4043/30775-MS.